Modeling Fe-Cr Alloys:
A Multiscale Approach

A thesis submitted towards partial fulfilment of
BS-MS Dual Degree Programme

by

Somil Gupta

under the guidance of

Dr. Mukul Kabir

Assistant Professor

Indian Institute of Science Education and Research
Pune

Certificate

This is to certify that this thesis entitled “Modeling Fe-Cr Alloys: A Multiscale Approach” submitted towards the partial fulfilment of the BS-MS dual degree programme at the Indian Institute of Science Education and Research Pune represents original research carried out by Somil Gupta at the Indian Institute of Science Education and Research Pune, under the supervision of Dr. Mukul Kabir during the academic year 2013-14.

Student
Somil Gupta

Supervisor
Dr.Mukul Kabir

Acknowledgements

Thanking my guide and mentor Dr. Mukul Kabir, would be an understatement.

I would like to thank my friend Rohit Babar for every instance of our discussions, and looking after me when I couldn't see through my attempts.

All the labmates (B215-B214) to kindly and happily bear with an extra (unassigned) occupant at their work-place. Sincere thanks. It was a very active and memorable learning with all of you.

My friends, Prashant Bhaskar, Adwiteey Mauriya, T.Harsha for making the final year memorable.

Abstract

With an aim of building next generation fission nuclear reactors with better reliability and efficiency, scientific community has shortlisted candidate structural materials which shall be tested exhaustively before they are taken up in the power industry. The research studies have established that Ferritic and Martensitic Fe-Cr alloy steels are the front-line candidate materials for the most promising of future reactor designs. These reactors would be serving in aggressive working conditions, with temperature range 300-900°C and neutron dosage of 15-150 dpa. These Fe-Cr alloys bring a number of advantages like void swelling resistance and relatively good corrosion and creep resistance in the profile of reactor steels. However, if we pursue them as it is, they still pose major technological hurdles for such extreme working conditions, and could be potentially disastrous.

A real-time experimental approach for these irradiation studies prove to be very expensive, and at times even inaccessible. Hence, modeling these structural materials through suitable approaches has been widely used to augment our understanding. In this thesis, we used a hierarchy of modeling techniques, which span different length and time scales of the underlying phenomena in these alloys. At the lowest order of this multiscale approach we investigated through density-functional theory calculations using plane-wave basis within VASP package, followed by nudged elastic band method for estimating the migration barriers of various activated processes, under the assumptions of Harmonic Transition State theory. Our results of these energetics is consistent with reported *ab initio* and experimental studies. These energetics are further taken to micro- and milli- length and time scales by kinetic monte carlo (KMC) simulations, whose code was developed by me for this work. This is tested using Einstein's equation of diffusivity over the range of 300-1500°C for vacancy migration in ferritic (bcc) Fe. This approach of studying the energetics of the dominant atomistic migrations which lead to diffusional transport, and later suitably accommodating these in the KMC code, could reveal the key mechanisms in the responses of material in reactor-like conditions. This would be very crucial to understand the underlying phenomena and design resistant structural materials to endure radiation damage.

Contents

Chapter 1

Introduction

1.1 Nuclear Power: An alternative for an energy secure world

The first nuclear reactor for civilian electricity generation came up in 1953 after the historic speech of “Atoms for Peace” by US President Dwight D. Eisenhower at the UN General Assembly. It was then, for the first time, when nuclear technology was talked about in public space to be disseminated for peaceful uses, like generating electricity. By the 1980s, 218 power had started up worldwide, with an average of about one reactor every 17 days [1]. However, soon along with the rise in investment in this industry there began one of the most lasting debates in the history of technology controversies. In April 1986, the catastrophic accident at Chernobyl power plant raised serious concerns regarding safety and reliability in using nuclear energy. This accident along with a slowdown of many economies leading to a very small rate of growth in energy demand, stalled the deployment of reactors in a number of countries around the world. Recently, the debate has further intensified after the accident in Fukushima plant in Japan (2011).

1.1.1 Enhanced safety and performance: The mission of next generation nuclear reactors

Inspite of such an environment of debate and doubt over this technology, many developing and developed countries have continued to take the alternative of nuclear energy seriously. Beginning from 2001, ten countries and European Union finally agreed on a framework of international cooperation in research for future nuclear energy systems, known as Generation IV International Forum (GIF). The mission laid out in this international science expedition is to design and develop next generation of nuclear power reactors with better sustainability, profitability, safety and reliability, and proliferation resistance. The scientific community has short listed six most promising designs of reactors from about hundred of them, for further exhaustive research regarding their feasibilty and implementation. These reactors would be required for unprecedented service conditions of high-energy neutron fluxes about 15 - 150 dpa along with intense thermomechanical stresses like core outlet temperatures of 350-900°C[2]. A chart of the candidate materials for the components of the future reactors is in figure 1.1.

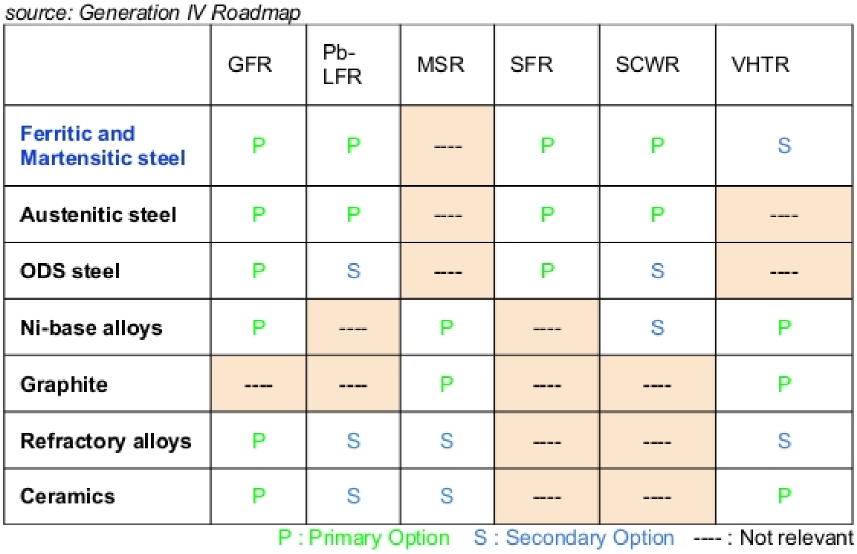

source: Generation IV Roadmap

	GFR	Pb-LFR	MSR	SFR	SCWR	VHTR
Ferritic and Martensitic steel	P	P	----	P	P	S
Austenitic steel	P	P	----	P	P	----
ODS steel	P	S	----	P	S	----
Ni-base alloys	P	----	P	----	S	P
Graphite	----	----	P	----	----	P
Refractory alloys	P	S	S	----	----	S
Ceramics	P	S	S	----	----	P

P : Primary Option S : Secondary Option ---- : Not relevant

Figure 1.1: Candidate materials for the shortlisted reactor designs Ferritic-Marensitic steels are the primary choice for a number of designs

1.1.2 Ferritic-Marensitc steels

These are body centred cubic (bcc) Fe based alloys with high (9-12%) Cr content, which offer a host of advantages over other candidate materials, like good resistance to damage accumulation, corrosion resistance, and lesser void swelling. However, before loading these structural materials with unprecedented neutron fluxes and temperatures in the future reactors, the response of these alloys have to be precisely understood, and further optimized. Moreover, many mechanical properties of the alloy are a non-monotonic function of Cr-concentration, leading to a conflict in trends of responses. Also, in severe working conditions the problem of Cr-phase segregation and radiation hardening pose a major embrittlement threat in using these materials. It is with these challenges in a multivariable space of thermophysical properties, dimensional stability, chemical compatibility, Cr-concentration, and all this - within a desired dosage of neutron fluxes and temperatures, the problem of structural materials design is poised.

1.1.3 Search for high-performance structural materials through modeling

On the other hand, over the last two decades, with superior modeling methods and high-performance computing, studying materials with unprecedented degree of control and characterization has been possible. These methods, today not only aim to complement with the experimental findings but have a unique predictive power of their own. Some of the central challenges of the current modeling approaches are: "achieving thermodynamical accuracy, bridging length-scales, and overcoming time-scales limitations"[3].

1.2 Multiscale Modeling Approach

The problem of failure in structural materials grows over multi-scales of length and time, and it needs to be understood how do the series of processes lead to each other. The underlying processes which result in such a heavy order of radiation damage span several orders of length($\sim$10 orders) and time ($\sim$22 orders)[4]. When the high energy neutrons collide with atoms of the alloy-matrix, it primarily knocks out few atoms, thus transferring most of their energy and further displacing other atoms by collision cascades. Such a cascade of displaced atoms cause various species of defects in the materials. Over time, these defects undergo a diffusional transport in varying environments, determining the evolution of microstructures at the order of hundreds of nanometres. Then, in the mesoscale regime various dislocation loops, thermomechanical stresses, irradiation creep and phase instabilities may emerge which, at macroscale, can even lead to unexpected embrittlement of components.

The objective of this approach is to acquire an appropriate micro- and meso-structural evolution of the material, after knowing the basic parameters governing the lower order processes in the length-time hierarchy. This requires feeding in of values of translatable parameters and key mechanisms from one model to another. The logic of connecting suitable models for simulating the real-processes is that they shall work with a consistent body of assumptions, and shall pass on results in the form of parameters to the next order of length-time scales.

It must be understood that a complete multiscale modeling of irradiation damage in alloys would be a huge task at hand, or even insufficient for prototyping the suitable structural materials; but only with such a bottom-up understanding of materials can we have deeper insights to understand and predict the responses while performing real tests and experiments.

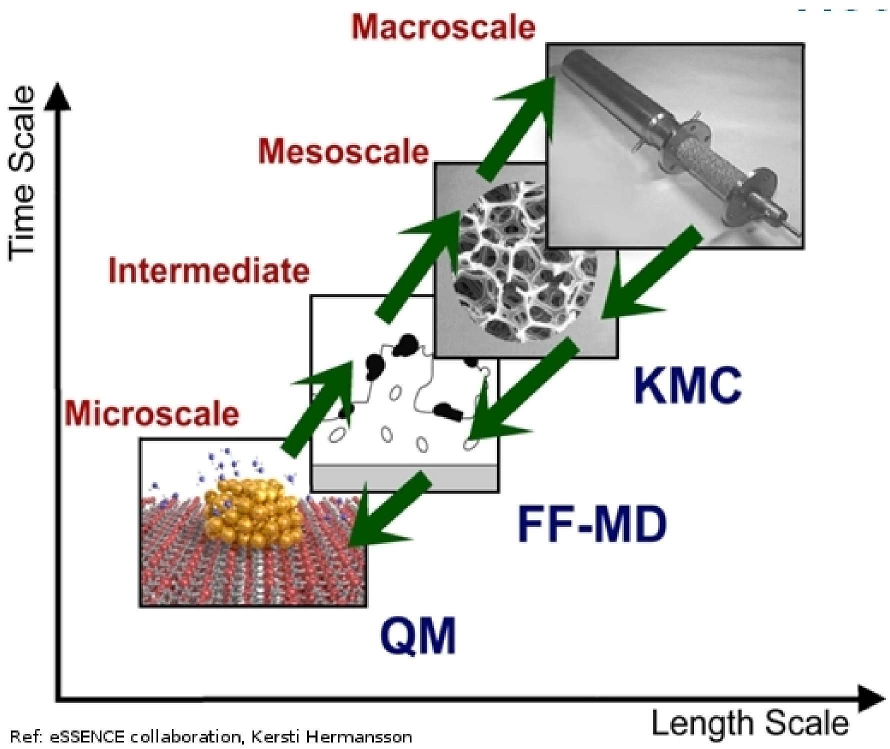

Figure 1.2: Multiscale materials modeling
A bottom-up approach to understand and engineer macroscale responses

1.3 Overview

In this thesis, we report our study of this alloy system to track down the effects of point defects in bcc Fe (along with substituted Cr), by spanning our study through atomic distances to greater than micro-scales. From section 2.1 - 2.2 I have briefly covered the developments in the way of solving the many-body Hamiltonian with the help of density-functional theory. In section 2.3 the method to find the minimum energy pathway and migration barriers for a process has been introduced, leading to the technique of nudged elastic band. Section 2.4 explains a framework of kinetic monte carlo technique to take the knowledge of these migration barriers to the next order of length-time scales in order describe the processes in terms of kinetics of the system. A simple code of kinetic monte carlo had also been built by me for this study which could accurately perform the vacancy diffusion in bcc systems.

Chapter 2

Theory and Methods

2.1 The Lowest Scale: Solving the Many Body Hamiltonian

A simple non-relativistic Hamiltonian for $\mathcal{N}$ interacting atoms with w electrons per atom is:

$$\mathcal{H} = \sum_{i=1}^{\mathcal{N}} \frac{\mathbf{P}_i^2}{2M_i} + \sum_{k=1}^{N} \frac{\mathbf{p}_k^2}{2m_k} + \sum_{i,i'<i}^{N} \frac{(we)^2}{|\mathbf{R}_i - \mathbf{R}_{i'}|} - \sum_{i=1}^{N}\sum_{k=1}^{N} \frac{we^2}{|\mathbf{R}_i - \mathbf{r}_k|} + \sum_{k,k'<k}^{N} \frac{e^2}{|\mathbf{r}_k - \mathbf{r}_{k'}|} \tag{2.1}$$

where, N = Total number of electrons in the system = $w\mathcal{N}$, and other terms have their usual meaning.

These terms are the kinetic energy terms of nuclei and electrons, ion-ion interaction term, ion-electron interaction term, and finally the electron-electron interaction term. To have an understanding of the electronic structure of such a system, in principle, one shall attempt to solve the time-independent Schrodinger equation of the above Hamiltonian. This theoretical recipe, though profound in its simplicity, is far from being of much practical use in finding and predicting properties of atoms, molecules and materials. The above Hamiltonian has a number of two-body interaction terms arising from the coulombic potential, which give rise to the many-body problem in physics. Until today it has turned out that, one of the important ways forward to the get best of our knowledge of quantum treatment of atoms and molecules is by making a set of systematic approximations in the terms of the Hamiltonian and attempting to tackle it.

2.1.1 Born-Oppenheimer Approximation

This preliminary approximation is made to decouple the ionic degrees of freedom from the electronic degrees of freedom. It is founded on the fact that there is many orders of difference in masses of an electron and ions, as each proton or neutron is around 1800 times heavier than an electron ($M_{ion} >> m_{elec}$). This difference directly results in the frequency of the vibration of electrons is much larger than that of the ions, and consequently a longer characteristic time scale of ions much greater than that of electrons ($\tau_{ion} >> \tau_{elec}$). Owing to this, one can resolve the analysis of the $\mathcal{N}$-interacting atoms problem into two independent problems, one of electrons moving under a fixed configuration of ions, and later using this to solve the ionic part.

$$\Psi(\{\mathbf{r}_i\}, \{\mathbf{R}_i\}) = \psi(\{\mathbf{r}_i\}; \{\mathbf{R}_i\})\phi(\{\mathbf{R}_i\}) \tag{2.2}$$

Thus this approximation requires us to solve the electronic problem by considering the ions at rest; thereby, taking us to the next challenge of the electron-electron interaction term in the electronic Hamiltonian.

2.1.2 Tackling the Electronic Hamiltonian: Interaction Term

From 2.1 one can write the electronic Hamiltonian as follows:

$$H_{elec} = \sum_{k=1}^{N} \frac{\mathbf{p}_k^2}{2m_k} + \sum_{k,k'<k}^{N} \frac{e^2}{|\mathbf{r}_k - \mathbf{r}_{k'}|} + \mathbf{V}_{ion-elec} \tag{2.3}$$

As famously known, the middle term of inter-electron interaction is the only two-body term in the above H_{elec}, and yet proves too untenable to offer any analytical solutions for most of the real-life systems. Gradually with increasing computational capabilities, numerical treatment of this equation coupled with further approximations were able to complement with experimental results and emerged as a powerful alternative. These ab initio methods are numerical methods of solving a many particle system with first principles of quantum mechanics along with their set of assumptions to deal with the inter-electron interaction term of H_{elec} and the form of electronic wave function. In those uncertain times, it was only these ab-initio methods which could establish the usefulness of quantum-theoretical techniques in everyday life.

2.1.3 The Breakthrough of Hartree-Fock and Its Limitations

In 1935, a landmark method of Hartree and Fock was built upon the simplest of approximations so as to solve for the Hamiltonian in 2.3. It is one of the first methods which aimed to self-consistently solve for systems electronic ground state within a variational principle. It uses a simple form of a Slater determinant for an N-electron wave function in terms of single-electron wave functions, and a mean-field approximation of potential for every electronic wave function. Such a form of the total wave function clearly neglected the coulomb correlation effects between electrons. Moreover, it was then soon realized, that the Hartree-Fock method would prove intractable to tackle the many-body problem for atoms greater than $\sim O(10)$. This is because, the computational effort scales too badly with the number of electrons in the system. This is what Walter Kohn calls "*the exponential wall*" of computing time and workload, which was encountered by the then traditional wave-function methods[5]. By the mid-50s, approaches to track the many-body problem were already facing a standstill for lack of any landmark development in circumventing this exponential wall of computation.

2.2 Density Functional Theory

Finally, it was the pioneering work of Walter Kohn and others in mid-1960s which derailed from the standard use of wave function as a state variable and attempted to describe the the system with ground-state electron density alone. This paradigm shift in approaching our N-particle problem, by a new basic parameter was a more visualizable 3-variable function of charge density n($\mathbf{r}$) instead of a 3N-variable wave function $\psi(\mathbf{r}_1, \mathbf{r}_2, \mathbf{r}_3, \cdots \mathbf{r}_n)$ gave a tremendous computational advantage.The density-functional theory (DFT) has its foundations on two theorems of Hohenberg and Kohn (HK) (1964) and Kohn and Sham (KS) (1965). The discoveries of the two foundational papers of DFT are as follows:

First HK Theorem, HK (1964): *Ground-state charge density completely characterizes the system*
The ground-state charge density n($\mathbf{r}$) of a bound system of interacting electrons in an external potential v($\mathbf{r}$) determines this potential uniquely (up to an uninteresting additive constant). It was demonstrated that there is a one-to-one map between external potential v($\mathbf{r}$) and the ground-state charge density n($\mathbf{r}$). That essentially meant, that for a fixed v($\mathbf{r}$) as there is a fixed n($\mathbf{r}$), its corresponding Hamiltonian and also its solution set of wavefunctions and energies are fixed by this density n($\mathbf{r}$). In effect, all quantities can be expressed as density-functionals, and therefore, characterizes the total system. The proof can be found in A.1

Second HK Theorem, HK (1964): *A variational theorem for ground state charge density was formalized*
In this theorem, HK proved the variational principle for finding the ground-state charge density amongst a set of allowable densities ñ($\mathbf{r}$) satisfying the natural constraints:

$$\widetilde{n}(\mathbf{r}) \geq 0, \tag{2.4}$$

$$\int \widetilde{\mathrm{n}}(\mathbf{r})\,\mathrm{d}r = N \tag{2.5}$$

As all properties of the system are functionals of its true charge density, HK defined a total-energy density functional $E(n(\mathbf{r}))$ for any trial density satisfying the above two constraints as:

$E_v(n(\mathbf{r})) = T(n(\mathbf{r})) + V_{ee}(n(\mathbf{r})) + V_{e-ion}(n(\mathbf{r}))$

In our simplest case when the only external field for the electrons is of that of ions, $V_{e-ion}(n(\mathbf{r})) = v(\mathbf{r})$

$\Rightarrow E_v(n(\mathbf{r})) = \int n(\mathbf{r})v(r)\,\mathrm{d}\mathbf{r} + \mathcal{F}_{HK}(n(\mathbf{r})),$

where, $\mathcal{F}_{HK}(n(\mathbf{r})) = T(n(\mathbf{r})) + V_{ee}(n(\mathbf{r}))$ is the universal functional since it is independent of external potential. This universal functional $\mathcal{F}_{HK}(n(\mathbf{r}))$ can be written as $\left\langle \Psi|\widehat{T} + \widehat{V}_{ee}|\Psi \right\rangle$ which contains the electron-electron interaction term, encapsulating our earlier problem.
It says, for any trial density ñ(r) satisfying 2.4 and 2.5, $E(n_0(\boldsymbol{r})) \leq E_v(n(\boldsymbol{r}))$ *where,* n_0*(r) is the true ground state density.*

KS (1965): *Formalized a set of self-consistent one-electron equations*
A set of partial differential, one-electron, self-consistent equations were derived without neglecting correlational effects. The challenge of dealing with the electron-electron interaction term was bypassed by dealing a corresponding problem for a non-interacting electron gas with the same ground state electron density $n(\mathbf{r})$ as that of true interacting system. This reference system was described by a set of single orbital wave functions $\{\Phi_i(\mathbf{r})\}$.
The KS equations which are solved self-consistently are as follows:

$$\left[-\frac{1}{2}\nabla^2 + v_{eff}(\mathbf{r})\right]\Phi_i(\mathbf{r}) = \epsilon_i\Phi_i(\mathbf{r}) \tag{2.6}$$

$$n(\mathbf{r}) = \sum_{i=1}^{N} |\Phi_i(\mathbf{r})|^2 \tag{2.7}$$

$$v_{eff} = v(\mathbf{r}) + \int \frac{n(\mathbf{r}')}{|r - r'|}\, \mathrm{d}\mathbf{r}' + v_{xc}(\mathbf{r}) \tag{2.8}$$

$$v_{xc} = \frac{\delta E_{xc}}{\delta n(\mathbf{r})} \tag{2.9}$$

These equations are solved consistently, by beginning with a trial density function and an approximated exchange correlation functional. Later using these functions according to equation 2.8 and 2.9 to get the respective v_{eff}, and use that to solve 2.6 for a set of single-orbital wave functions. This set can be further used to calculate the charge density. If this charge density comes to be the same as the input-fed charge density we say the solution is self-consistent, and consider that to be the charge density of the ground state. If this is not the case, we proceed with such reiterations by changing the charge density. The key advantage derived with KS equations is able to get $T_s(n(\mathbf{r})$ (K.E term of non-interacting gas) which is a dominant part of the kinetic energy $T(n(\mathbf{r})$ (interacting term of interacting gas), leaving the E_{xc} to be searched. If the exact E_{xc} were known, one would have the exact $n(\mathbf{r})$ and the exact $E(n(\mathbf{r}))$. Hence, to effectively apply the above theorems, one needs to construct exchange-correlation functionals which can be further be successively improved. Though remarkable progress have been made in this, it still remains to be the real great challenge in applying DFT.

2.2.1 Exchange-Correlation Energy Functionals

The theoretical framework of DFT could be brought under practice only after a hierarchy of approximate Exchange-Correlation Energy functionals were developed, after the pioneering work of Perdew, Becke and Ernzerhof [10]. These functionals are an indispensable necessity without which DFT could not have been applied effectively. Examples: LDA, GGA, meta-GGA, Hyper-GGA, Hybrid functionals.

Local Density Approximation (LDA): Although it is the simplest of approximations of density functionals, it has proved very efficient in DFT calculations. It says that the energy functional can be constructed by assuming that the exchange-correlation energy per electron at a point $\mathbf{r}$ in the interacting electron gas equal to that in a homogeneous electron gas with same charge density. Hence, it ignores corrections to the exchange-correlation energy at a point r due to nearby inhomogeneities in the electron density.

$$\mathbf{E}_{xc}^{LDA}(n(\mathbf{r})) = \int_{0}^{\infty} n(\mathbf{r})\mathcal{E}_{xc}^{LDA}(n(\mathbf{r}))\,\mathrm{d}^3\mathbf{r} \tag{2.10}$$

where, $\mathcal{E}_{xc}^{LDA}(n(\mathbf{r}))$ is the exchange plus correction energy per electron in a homogeneous electron gas with electron density $n(\mathbf{r})$. Hence, $\mathcal{E}_{xc}^{LDA}$ would not include the effects due to inhomogeneities in the electron density.

Generalized Gradient Approximation [GGA]: It assumes dependence of the exchange-correlation energy on local electron density; as the functional is assumed to depend on density and its gradient. It has the form:

$$\mathbf{E}_{xc}^{GGA}(n(\mathbf{r})) = \int_{0}^{\infty} n(\mathbf{r})\mathcal{E}_{xc}^{GGA}(n(\mathbf{r}), |\nabla(n(\mathbf{r}))|)\,\mathrm{d}^3 r \tag{2.11}$$

where, $\mathcal{E}_{xc}^{GGA}(n(\mathbf{r}), |\nabla(n(\mathbf{r}))|)$ is the exchange plus correction energy per electron depending on $n(\mathbf{r})$ and $\nabla n(\mathbf{r})$. It may seem, that as $E_{xc}^{GGA}(n(\mathbf{r}))$ include more information than $E_{xc}^{LDA}(n(\mathbf{r}))$ it would always be more accurate. This however may not be the case, as there are many ways to incorporate the information of the gradient of the electron density in the GGA functional, resulting into a large number of them. As these functionals are produced for single isolated molecules, it becomes imperative to clearly mention the E_{xc} functional which have been used for a DFT calculation.

2.2.2 Bloch Theorem

It remains a problem that a basis set, required to expand each electronic wave function in bulk solid would be infinite. Bloch theorem proves to be the starting point in surmounting this problem. It states that in a periodic solid, each electronic wave function can be written as a product of a cell-periodic part and a wave-like part:

$$\psi_{i,k}(\mathbf{r}) = e^{\mathbf{ik.r}}\mathcal{F}_i(\mathbf{r}) \tag{2.12}$$

where the subscript i indicates the band index and $\mathbf{k}$ is a continuous wave vector that is confined to the first Brillouin zone of the reciprocal lattice. The cell-periodic part which has the same periodicity as the direct crystal, is expanded in a basis set consisting of discrete set of plane waves, whose wave vectors are reciprocal lattice vectors of the crystal.

$$F_i(\mathbf{r}) = \sum_{i,G} c_{i,G}\; e^{\mathbf{iG.r}} \tag{2.13}$$

Using 2.12 and 2.13, an electronic wave-function at each $\mathbf{k}$-point can be expanded in terms of a linear combination of plane waves.

$$\psi_{i,k}(\mathbf{r}) = \sum_{i,G} c_{i,k+G}\; e^{\mathrm{i}(\mathbf{k}+\mathbf{G}).\mathbf{r}} \tag{2.14}$$

2.2.3 K-point Sampling

In a practical plane wave DFT calculation, many a times one faces with challenge of evaluating the integrals of the form: $\int\limits_{BZ} f(\mathbf{k})\,\mathrm{d}\mathbf{k}$.
To overcome this problem, the integrations can be performed as summations over a finite, but sufficiently dense mesh of k-points - instead of actual integrals in the continuous space:

$$\int\limits_{BZ} f(\mathbf{k})\,\mathrm{d}\mathbf{k} = \frac{1}{\Omega}\sum_{j} w_j f(\mathbf{k}) \tag{2.15}$$

where, Ω is the cell volume and w_j are weighting factors.
This method entails calculating the periodic functions at an infinite number of points in reciprocal space, which will be referred to as **k**-points. With these infinite **k**-points we exploit the fact that electron wave-functions do not change appreciably over small distances in **k**-space. Hence, it becomes possible to expand these wave-functions over a region of **k**-space by the wave-function at a single **k**-point.

The number of **k**-points required for a sufficiently accurate calculation must be ascertained by **k**-point sampling - a procedure in which the total energy of the system is converged with respect to increases in the **k**-point mesh density. Also, the error in the total energy due to inadequacy of **k**-point sampling can always be bettered by using a denser set of **k**-points.

2.2.4 Plane Wave Basis Set

The Bloch theorem in 2.14 enables one to expand the electronic wave function in an infinite and discrete plane-wave basis set. According to this expression, evaluating the solution at even a single point in **k**-space would involve a sum over an infinite number of possible values of **G**. However, it is found that the plane-wave coefficients $c_{i,\mathbf{k}+\mathbf{G}}$ for lower kinetic energy are typically important than those with large kinetic energies. That gives us a justified ground to truncate this expansion of plane-waves, after a suitable cut-off energy, where the results of the calculation converge as follows:

$$\psi_{i,k}(\mathbf{r}) = \sum_{i,|\mathbf{G}+\mathbf{k}|\leq G_{cut}} c_{i,k+G}\; e^{\mathrm{i}(\mathbf{k}+\mathbf{G}).\mathbf{r}} \tag{2.16}$$

One of the advantages of using a plane-wave basis is the convenience of making a systematic improvement in reducing errors due to truncation, by including successive terms in the expansion. This energy cut-off, depends on the system at hand, i.e. the pseudopotentials chosen to describe the system.

2.2.5 Pseudopotential Theory

It exploits the fact that most of the physical properties of solids are dependent on the valence electrons alone. It does this by replacing the chemically inert core electrons and the strong ionic potential by a weaker pseudopotential that acts on a set of pseudo wave-functions than the true valence electrons. The focus on nodeless valence electron wave-function instead of all-electron system helps tremendously in reducing the computational load of managing a strong potential. As this weaker substitution for ionic potential and valence electrons allows a smaller set of plane waves in the basis, pseudopotential theory complements well with the plane-wave method. It shall be noted that the only criteria for a good pseudopotential is how well it matches the results of all-electron experiments.

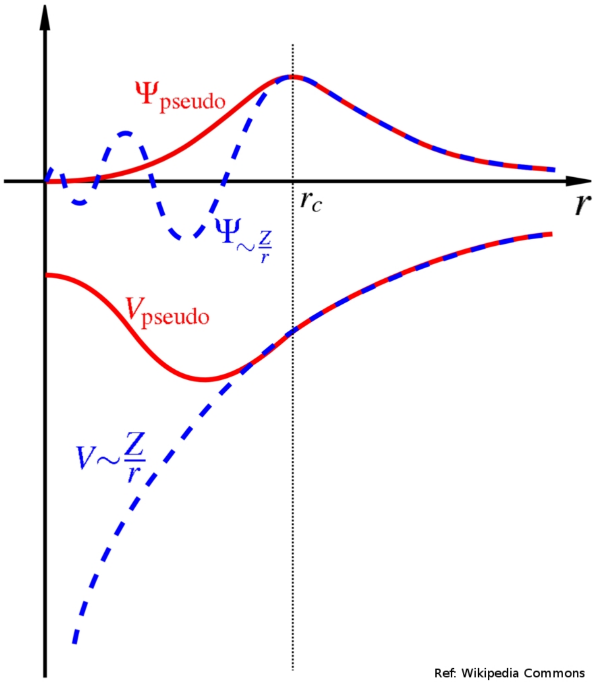

Ref: Wikipedia Commons

Figure 2.1: Approximation to ionic potential and all-electron wavefunction
Beyond a cut-off radius r_c, the pseudopotential and the pseudo-wavefunctions have exactly same behaviour

2.3 Activated Processes

At the next level of hierarchy in our multiscale modeling we use the ground states from optimized DFT calculations to simulate what are known as *activated processes* - which at some point of their reaction trajectory pass through configurations of higher energy than the initial reactant configuration. In this process the trajectory which requires lowest energy increments at every step of reaction pathway is called the Minimum Energy Path (MEP). Also, for any point on the MEP the forces point only along the trajectory. It equivalently means that any point on the MEP is at an energy minimum in all other directions perpendicular to the reaction pathway [6]. The point on this trajectory which is a first order saddle point is called the transition state, and the energy difference between the transition state and the reactant configuration is the migration barrier of the activated process. Modeling of such processes holds tremendous value in tracking the evolution of the solid-state diffusive systems. Examples of these processes are diffusion events in crystals, or on a surface, passage of a catalytic reactions, etc.

2.3.1 Time-Scale Problem of Activated Processes

It turns out that an attempt at modeling of such activated processes of real interest by the direct classical molecular dynamics (MD) approach is severely restricted by the accessible timescales of the MD (∼ns). The key problem with such activated processes is that their occurrence is relatively rare in comparison to molecular vibrations. For example, even to simulate a process having an activation barrier as low as 0.6eV (a typical diffusion barrier on surfaces) at room temperature, it would take about 10^5 years of computing time on present day computers. This is because, statistically to witness one such diffusive event there would have to be about 10^{10} molecular vibrations which a MD simulation would have to resolve to track an appropriate evolution of the system[7]. However, the time scale problem is herculean for the dynamical approach but makes it possible to obtain accurate estimates of transition rates only after resorting to a statistical approach of transition state theory.

2.3.2 Harmonic Transition State Theory

An important formulation in understanding these activated processes is of a rate constant which characterizes the probability per unit time of occurrence of the activated process depending on its energy barrier and temperature of the equilibrium ensemble. Eyring's pioneering work of Transition State theory (TST) in 1935 laid the ground for treating these processes by an important assumption that the transition states are in thermal equilibrium with the reactants. Later in 1957, G.H Vineyard added on to the assumptions of TST and formulated a theory which proves very more convenient and less error prone in calculating these rate constants, called the Harmonic Transition State theory (HTST). In HTST, apart from a Boltzman population one uses the theory of small vibrations and assumes that near a basin on potential energy surface, energy could be expressed up to a second-order expansion.i.e, the vibrational modes are harmonic - and that holds even for the first order saddle point for the modes perpendicular to the reaction coordinate[8]. The rate constant is defined as in equation below using the equilibrium fluxes through a dividing hyperplane passing through the saddle point and perpendicular to reaction coordinate, in the configuration space 3N dimension (N is the number of atoms in the system).

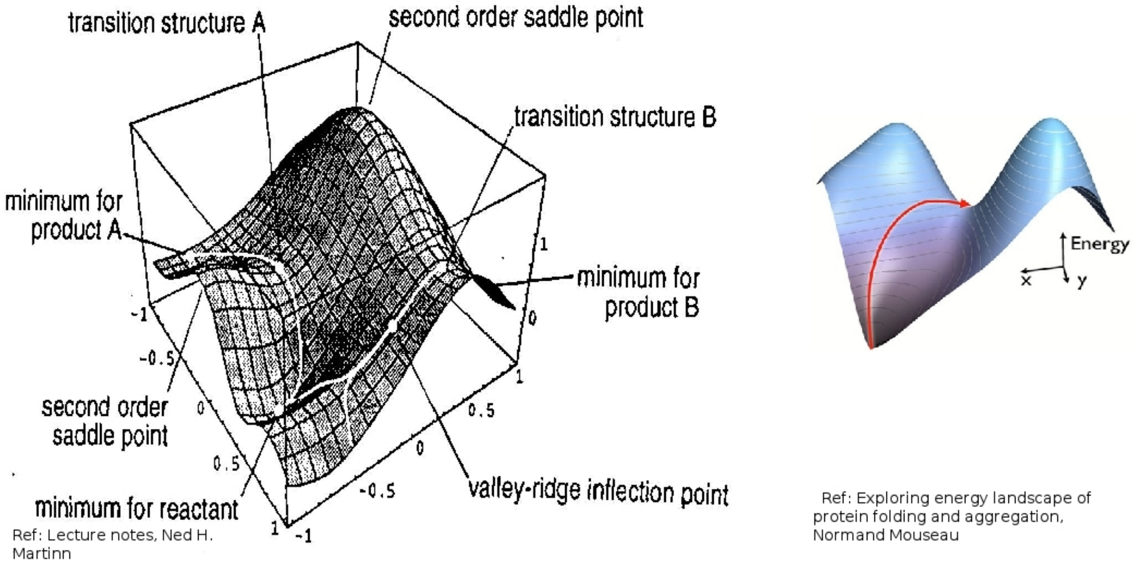

Ref: Lecture notes, Ned H. Martinn

Ref: Exploring energy landscape of protein folding and aggregation, Normand Mouseau

Figure 2.2: MEP: as a first order saddle point on the PES
The hyperplane is perpendicular to the MEP at the saddle point

$$k_{HTST} = \frac{I}{Q}; \tag{2.17}$$

where Q is number of representative points in the configuration space in the part of the region between reactant and transition state, and I is number of representative points in the configuration space crossing the transition state from reactant side to the product side.
As the transition state is a first order saddle point on the potential energy surface (PES), it has exactly one imaginary frequency (along the direction of the reaction coordinate for which it is a transition state). Hence the remaining normal modes, 3N-1 are non-imaginary. Through HTST, Vineyard proved that the calculating the rate constant only requires the information about the reactant and the transition state along the reaction pathway; and derived the rate constant to be:

$$k_{HTST} = \left(\frac{\prod_{i=1}^{3N} \nu_i^{reac}}{\prod_{j=1}^{3N-1} \nu_j^{sad}} \right) \exp(-\frac{E_{mig}}{k_b T}) \tag{2.18}$$

The prefactor contains ν_i^{reac} are the 3N normal mode frequencies at the reactant basin, ν_j^{sad} are the 3N-1 non-imaginary normal mode frequencies at the saddle, and E_{mig} is the migration energy barrier.
The calculation of the prefactor is done by a standard and cumbersome routine. They are generally in the range $10^{12} - 10^{13}$, and as an approximation they are taken to be a fixed value in the above range to save the computational load of evaluating the normal modes for every transition state for every reaction pathway. It has been seen that k_{HTST} proves to predict the rates to very good accuracy and are widely used in the diffusive solid-state process up to at least half the melting point[9].

2.3.3 Techniques for Finding the Transition State of the Reaction Pathway

Clearly, the k_{HTST} requires considerable information from the saddle point to find the rate constants. However, it turns out finding a saddle point for a given pair of initial and final configurations is a real challenge. Moreover, to find the rate constant k_{HTST} for a process it would require the highest energy saddle point along the pathway, if more than one saddle point lie occur on the MEP. As mentioned in section NEB, the transition state being a first order saddle point on a MEP has a maxima in only one direction and an energy minimum in all other directions, methods for finding transition states invariably involve some kind of maximization of one degree of freedom and minimization in other degrees of freedom. The critical issue is to find an inexpensive estimate of which degree of freedom should be maximized.

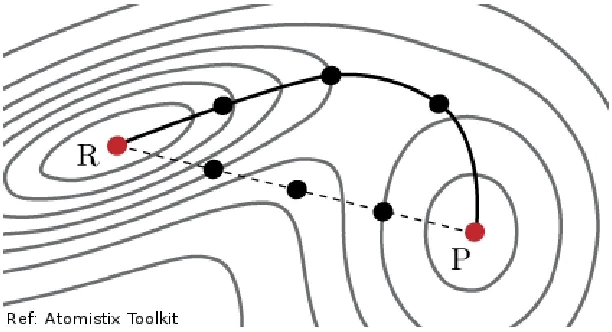

Ref: Atomistix Toolkit

Figure 2.3: A set of images produced by linear interpolation using reactant and product, which are finally converged to the MEP

2.3.4 Nudged Elastic Band Method

It is a type of chain-of-states method where a series of images (configurations of the system) between the initial and final optimized states of the transition, are constructed and used to optimize the pathway to a MEP using a force projection scheme. Let the initial and final optimized images, which form a basin in the PES, be called r_0 and r_N; and the series of images which represent a systematic development of the states from r_0 to r_N are identified using a linear interpolation and called $r_1, r_2 \cdots, r_{N-1}$. Most of the intermediate images are naturally driven to either basin of r_0 or r_N of the PES; except when they are at a saddle point of the PES. To restrict these intermediate images to fall into either of the basins a constraint needs to be imposed on these images. This is brought in by adding an artificial harmonic spring force term which is negative of gradient of a constructed spring energy of $k(r_{i+1} - r_i)^2$. Here k is called the spring constant and the corresponding force is given by: $\mathbf{F}_i^s = k(|r_{i+1} - r_i| - |r_i - r_{i-1}|)\widehat{\tau_i}$

The images are made to converge to MEP under a force projection of:

$$\mathbf{F}_i|_\perp = -\nabla E_i|_\perp \quad + \quad \mathbf{F}_i^s|_{||}\widehat{\tau_i}.\widehat{\tau_i} \tag{2.19}$$

and the NEB condition is $\mathbf{F}_i|_\perp = 0$. Consequently, a NEB calculation facilitates a good estimation of the MEP and the transition states in the reaction pathway.

However, with this much at our disposal, we can get only a qualitative picture about which migrations are dominant and which are less probable, but would not be able to usefully predict about systems dynamical evolution in higher order of length and time scales.

Ref: Optimization methods for finding minimum energy paths, Daniel Sheppard

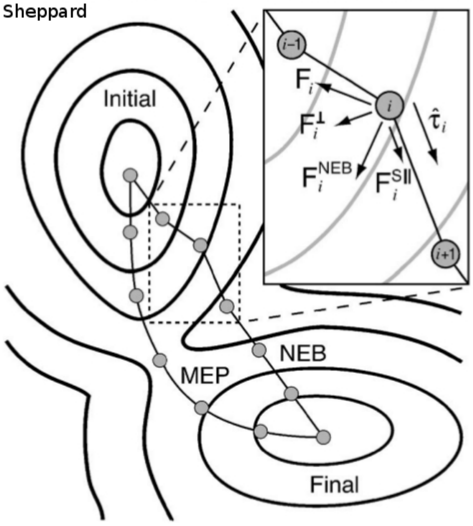

Figure 2.4: Force projection scheme used by NEB for optimizing the MEP

2.4 From Atomistic Migration to Diffusional Transport

A benchmark technique to propagate the system in time has been classical Molecular Dynamics which uses equations of motion, for suitable interatomic potentials and appropriate boundary conditions. However, as the idea requires resolution up to atomic vibrations to direct the system's evolution it becomes enormously difficult to reach timescales more than a microsecond [9]. This time scale problem, which was also mentioned in section 2.3.1, limits one to reach further higher orders in timescales ($10^{-5} - 10^{3}s$), which prove to be a crucial bridge between atomistic understanding and macroscopic predictions about the system. Kinetic Monte Carlo method exploits this long-time-scale problem by using a probabilistic description and the knowledge of the energetics of the system to describe its evolution under HTST and other assumptions.

State of the system: KMC uses diffusion from one *state of the system* to another. These states are configurations of the system which are basins in the PES of configurational space of the system. If due to external perturbations in energy of a system, it gets excited but still remains to be the part of the same basin - it is referred as the same state of the system as earlier. Any change of state essentially means a change in basin by crossing an energy barrier. It is such state-to-state jumps which evolve the system in the KMC procedure. So, system in state i would have probabilities of transition per unit time, k_{ij} to escape to any of the other state j of the system. It is observed that the probability distribution of system to have survived in state i is a first-order rate process and can be shown to have the following dependence of:

$$P_{survival}(t) = exp(-k_{tot}t) \tag{2.20}$$

where $k_{tot} = \sum_j k_{ij}$, denotes the total escape rate per unit time from state i.
The probability distribution of the first escape $p(t)$ from this state i can be derived from $P_{survival}$ as follows:

$$\int_0^t p(t')\,\mathrm{d}t' = 1 - P_{survival}(t) \tag{2.21}$$

on further differentiation under an integral, we get:

$$\implies p(t) = k_{tot}exp(-k_{tot}t) \tag{2.22}$$

And, such a first-passage distribution is found for every transition pathway between states i and j.

$$p_{ij} = k_{ij}exp(-k_{ij}t) \tag{2.23}$$

Markov process: The key feature of KMC is in assuming the transition event, an occurence irrespective of system's history and the course of pathways through which it has reached its current state. This property in a makes up a unique class of processes called Markov processes, which has a topic of research in itself. It is a reasonable assumption to make for solid state atomistic systems where events are highly infrequent in nature; and, thus can be understood to have *lost their memory* of how it entered the state on a timescale that is short in comparison to the time intervals between the transition events. This assumption enables the transition probabilities to be constants of time for any give pathway. To use this method, one requires to calculate rate constants for different possible migrations for a given state from equation 2.18, using the migration energies from NEB, and using an approximate prefactor of $\sim 10^{13}$Hz. A simple type of algorithm for KMC is given as follows:

2.4.1 KMC Algorithm and Motivation

A type of KMC (residence-time) algorithm:

---

1. Set **Time (t) = 0**
2. Make a catalog of all transitions events possible from the current state i and their rate constants k_{ij}
3. Calculate a cummulative function $K_j = \sum_{i=1}^{j} k_i$ for j = 1, 2, $\cdots$, N, where N is the number of total transition events possible from the current state
4. Generate a uniform random number, uϵ (0,1]
5. **Select the event** i to be carried out, from the list of possible events by the condition:

$$K_{j-1} < uK_N \leq K_j$$

*Note: K_N denotes the total escape rate constant = k_{tot}
6. Carry out the selected event j
7. Get a new uniform random number u$'$ ϵ (0, 1]
8. **Update the Time** t = t + Δt, where $\Delta t = -\frac{1}{K_N} ln(u')$
9. Again make a list of all possible events which could be take place from the new state, and **repeat the process for number of KMC steps**

The conceptual basis of the procedure is to have a stochastic method that will propagate the system from one state to another, keeping in considerations their first passage rate constants and the total escape rate constant [9].
An event is such selected that the probability of choosing an event is propor-

tional to $\frac{k_{ij}}{R}$, and can be understood from figure 2.5.

By using 2.21 it can be easily verified that the average time for escape τ is

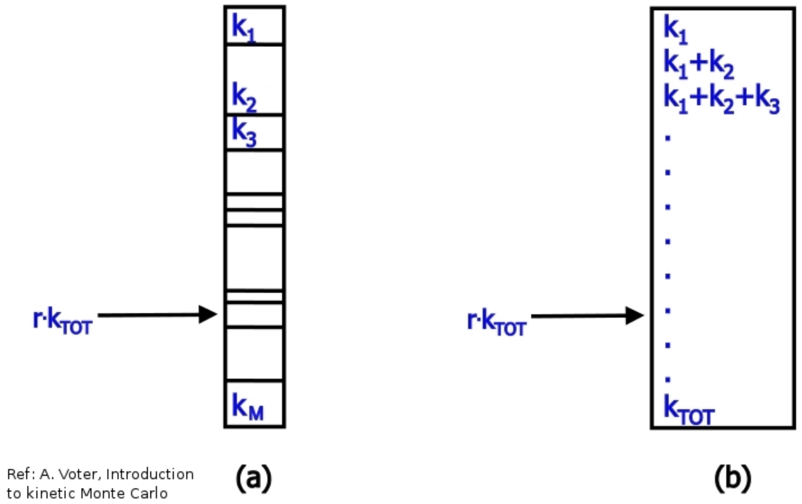

Ref: A. Voter, Introduction to kinetic Monte Carlo

Figure 2.5: Choosing an event for a KMC step: It can be understood from (a) and (b) that chances of an event getting selected is proportional to $\frac{k_{ij}}{R}$

just $\int\limits_{0}^{\infty} tp(t)\,\mathrm{d}t = \frac{1}{k_{tot}}$. Also, the average of $ln(u')$ over $u'\epsilon(0,1]$ is -1; making the average time increment of Δ t $= \frac{1}{k_{tot}}$ thus, giving an appropriate average time for an event to occur. The random number in time increment is to include stochasticity of the real process, and yet not to change the average time for escape.

2.4.2 Limitations and Challenges of KMC

The basic crucial input required for KMC is the catalog of rate constant of all *possible* transitions. That leaves quite a gap to be certain of the predictions of the KMC as one might never be sure if a possible event has been left out. This is the limitation of using KMC as the real dynamical evolution might not be made up of simple events, and we might not be able to include them in our rate catalog in the simulation. This challenge has further led to newer modeling methods.

Chapter 3

Tools

3.1 DFT and NEB calculations: VASP software package

Vienna Ab-initio Simulation Package (VASP)[1] was used for my DFT and NEB calculations. It provides a method for a DFT calculation with plane-wave basis set, periodic boundary conditions, PAW[18][19], and Monkhorst-Pack scheme[15]. The source code is written in Fortran 90. The NEB method written by Henkelman[6] group could be used by simply compiling within VASP.

3.2 My Kinetic Monte Carlo Code in C

To effectively use and accommodate the variety of defect species, it becomes imperative to build KMC code for the problem at hand. I have worked out my code for a simple case of vacancy diffusion in bcc geometries. The code can be found in A.2

3.2.1 Input Parameters:

- Number of Atoms to be simulated
- Percentage of vacancies
- Percentage of Cr
- Temperature of the simulation
- Migration energy barriers (calculated by NEB) relevant to all the activated process which are being considered

[1] VASP was written by Prof. Mike Payne at MIT, and has the same roots as CASTEP.

3.2.2 Features of the code:

- Makes a bcc geometry with required number of atoms
- Creates a certain percentage of vacancies and Cr by a random number generator, in such a way that no two of them have the same lattice site
- Finds the first nearest neighbours of all lattice sites within the periodic boundary conditions. Also, with the knowledge of the species (atoms/defects) occupying this neighbourhood
- Makes an event table for every state of the system along with rate constants for all possible migrations to the first nearest neighbourhood
- One of the event is chosen among all the possible events for a given state of the system (using steps **3, 4 and 5** in 2.4.1)
- Calculates squared displacement for every migration. Though, this is same for all the jumps of 1nn vacancy diffusion, it has been done for a general case of migration
- Propagates the simulated time of the system (by step **6** in the 2.4.1)

3.2.3 Output:

- Mean squared displacement versus propagation of time for every migration
- Position coordinates of every state accessed to facilitate the visualization of the kinetics using AtomEye[2]

[2] AtomEye is a visualization tool developed by Ju Li, at MIT, used for a large system of atoms.

Chapter 4

Results and Discussion

Here, I report my results of modeling body centred cubic (bcc) Fe system with Cr as a solute; alloys of which have emerged to be the frontline candidate materials for working in aggressive conditions. The aim of my study is to model their kinetics which prove important in understanding the underlying atomistic events, microstructural evolution, and processes shaping the alloys profile. In this multiscale approach, I used DFT-based plane wave calculations on VASP, followed by studying the rate constants of various migrations through the NEB method under HTST assumptions. Finally, as a KMC code prerequires the specific details of the type of defects and geometry of the system, I have developed a KMC code for further study of kinetics of vacancy diffusion in a bcc geometry. It has been tested for this simplest case, and further would be worked upon to accommodate the kinetics of variety of other defects whose interaction with solute atoms play a significant role in these alloys.

4.1 Ab-Initio Results within DFT

In these calculations, as earlier mentioned in 2.2, various theoretical frameworks and approximations were integrated together. My calculations in VASP are performed specifically using supercell technique, **k**-point sampling of Brillouin zone within Monkhorst-Pack scheme [15], plane augmented wave method [18, 19] and exchange correlation functional [10]. The approximations made in **k**-point sampling and basis expansion can be systematically improved, but only with an additional expense of computational resources. However, for a fixed E_{xc} the calculations can be made to converge within desired accuracy; and when achieved is known as a numerically converged a DFT calculation.

4.1.1 Body Centred Cubic Structure of Fe and Cr

Below 1200 K the crystal structure of iron is known to be a ferromagnetic bcc geometry which makes up the solvent matrix of ferritic alloys (α-phase)[12].

In estimating the equilibrium lattice constant of this structure we use the fact that the real lattice constant of the system is the one which is the minima of energy (as an empirical function of geometry). In practice, this is done by studying a fixed-volume total energy calculation of a 2-atom bcc geometry for various lattice constants within a range of values as shown in figure 4.1(a) within periodic boundary conditions (built-in in VASP). Systematically, for a range of lattice constants, energy and magnetization was calculated as in figure 4.2. Experimentally, it is reported [11] that in bcc Fe the lattice constant is 2.87 Å and magnetic moment per atom is $2.2\mu_B$. Our calculations give results consistent with this fact, and give the values of 2.83 Å and $2.2\mu_B$, which are also in agreement with the reported ab initio values, considering the difference of E_{xc} and density of **k**-point mesh [12, 13, 14]. This can be understood from figure 4.2, where the 2-atom bcc cell of lowest energy is the one which has magnetic moment (per atom) as $\sim 2.2\mu_B$

An idea about the stability of a configuration can be derived by system's binding energy. The total binding energy is defined as the difference in energy when the entities interact and when they are isolated: $E_{interact} - E_{isolated}$.

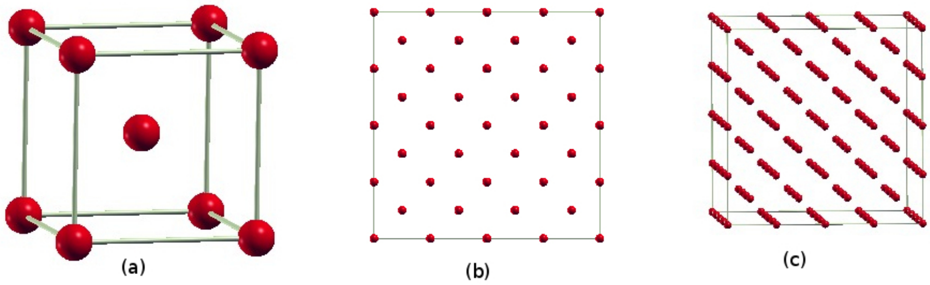

Figure 4.1: bcc Fe as viewed in XCrysden (a) Fe primitive cell of 2 atoms (b)and(c)*Front and Side view*
Supercell of 128 bcc Fe atoms of 128 bcc Fe atoms

Table 4.1: Lattice constant, Magnetic moment and Binding energy data of 128 bcc Fe atoms

Case	My Results	Olsson [14]	Domain [12]	Expt. [11]
Lattice Constant (Å)	2.833	2.831	2.852	2.87
Magnetic moment per atom (μ_B)	2.20	2.21	2.32	2.22
Binding Energy per atom (eV)	-4.85	- - -	- - -	-4.28

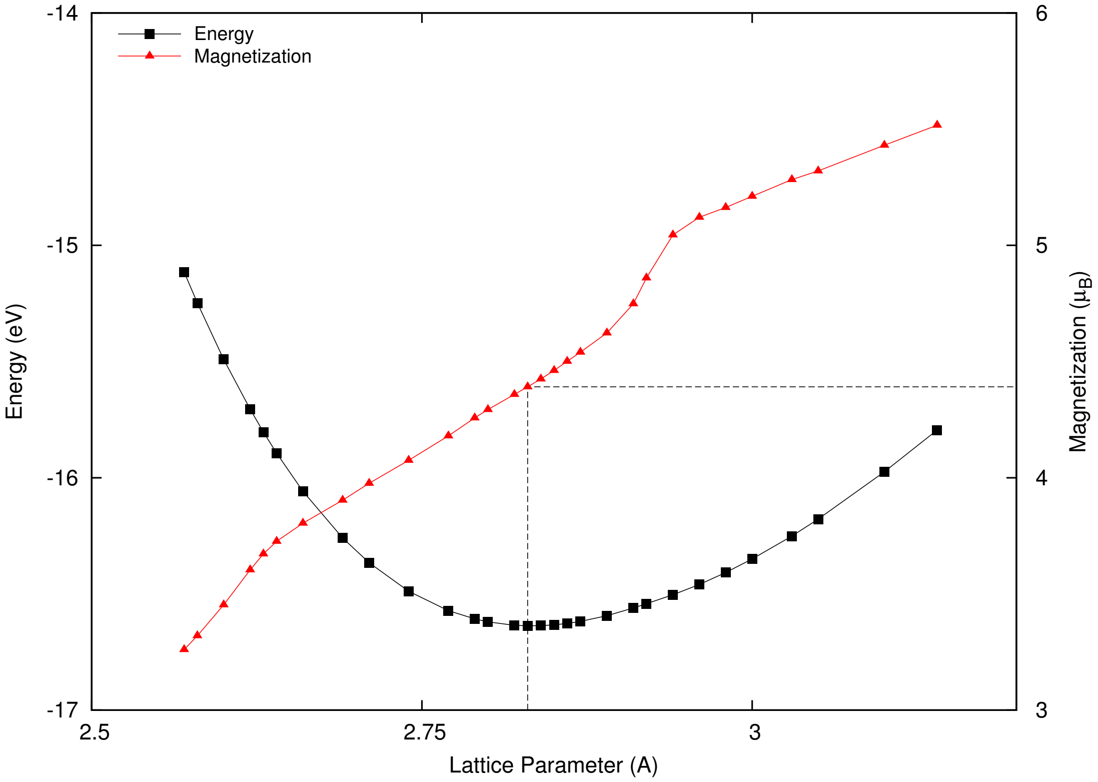

Figure 4.2: Energy vs Lattice constant for a 2-atom bcc Fe cell
At the minima of energy curve the magnetic moment of the cell is $4.39\mu_B$ (i.e., $2.195\mu_B$ per atom)

Formally, for the 128 atom supercell of bcc Fe, we can write:

$$\text{Binding Energy per atom} = \frac{[E_{128Fe} - 128E_{singleFe}]}{128} \tag{4.1}$$

The observed values of lattice constant, magnetic moment and binding energy per atom for the equilibrium lattice of 128 Fe atoms in bcc geometry are reported in Table 4.1. As the atomic radius of Fe and Cr is almost similar, so would be their lattice constants in the same geometry. The lattice constant of bcc Cr is found to be 2.836 Å and nonmagnetic, as reported earlier[14]. It shall be noted that though the reported magnetic structure of Cr and Cr-rich alloys is found to be complicated[16], we have restricted our attention to its nonmagnetic structure owing to its low N'eel temperature of 311 K, and for the application of high temperature working conditions can be considered as nonmagnetic. The binding energy of Cr is found to be about 4.03 eV/atom in excellent agreement with reported experimental value of 4.10 eV/atom [11].

4.1.2 Cr Substitution Defect in bcc Fe

For a composite system, formation energy of a defect indicates the difference in energy after and before the defect arises. Formally, for a system of n Fe atoms and p Cr atoms, it is defined as:

$$E_{form}(nFe + pCr) = E(nFe + pCr) - nE(Fe_{bcc}) - pE(Cr_{bcc}) \tag{4.2}$$

where, the terms on the right correspond to binding energy of the composite system (with substitution), binding energy per atom in bcc Fe supercell of same size, and the binding energy per atom in non-magnetic bcc Cr respectively. Here, the binding energy of a composite system means as earlier defined, i.e., the difference between total energy and the isolated energies of corresponding number atoms. The formation energies of a defected configuration indicates how easy it is to form that defect in a pure system. Figure 4.3 reports the observed data for formation energies of Cr substitutional defects in bcc Fe. Our calculations are concurrent with an important observed phenomena in Fe-Cr alloys: that, in low concentrations of Cr (<9%) the solute atoms tend to remain farther away from each other, at higher Cr concentration (∼9-10% Cr) homogeneous ordering of the alloy solution emerges, and further increasing Cr concentration, results in preferential Cr-Cr affinity; thus allowing formation of Cr-rich α'-segregation [17, 25, 26]. From figure 4.3 we can observe that comparing configurations (a), (b) and (c) (1.6 at.% at. Cr), also (d), (e) and (f) (2.3 at.% Cr) are in a decreasing order of formation energies, implying an ease of formation with increasing Cr-Cr distance in low Cr-concentration regime.

Also, it was observed that on substituting one Cr atom in bcc Fe matrix, Cr is antiferromagnetically coupled to the Fe atoms. On this substitution, magnetic moments of neighbouring Fe atoms does not change significantly. Only the Fe atoms, which are 1nn-to-Cr, show a decrease of $0.01\mu B$. Further, on substitution of more Cr atoms reduces the magnetic moment of Cr, as this explains the change in environment from bcc Fe to bcc Cr for that single Cr atom. In figure 4.3 comparison within (a), (b) and (c) shows how the local magnetic moment of Cr atoms gets restricted beside Cr atoms. The same can be seen in (d), (e) and (f). This results are in concurrence with the results [17] where, it was demonstrated that this magnetic interaction is the cause of preferred ordering of the atoms in going from low-to-high Cr concentration. We haven't verified the the effects at high Cr concentration, and hence, predictions and comparisons can be drawn only in this low concentration regime.

4.2 Vacancy Defects and NEB Results

The point defect (vacancies, interstitials or substitutions) play a crucial role in the kinetics in an alloy system, and their understanding would be necessary to

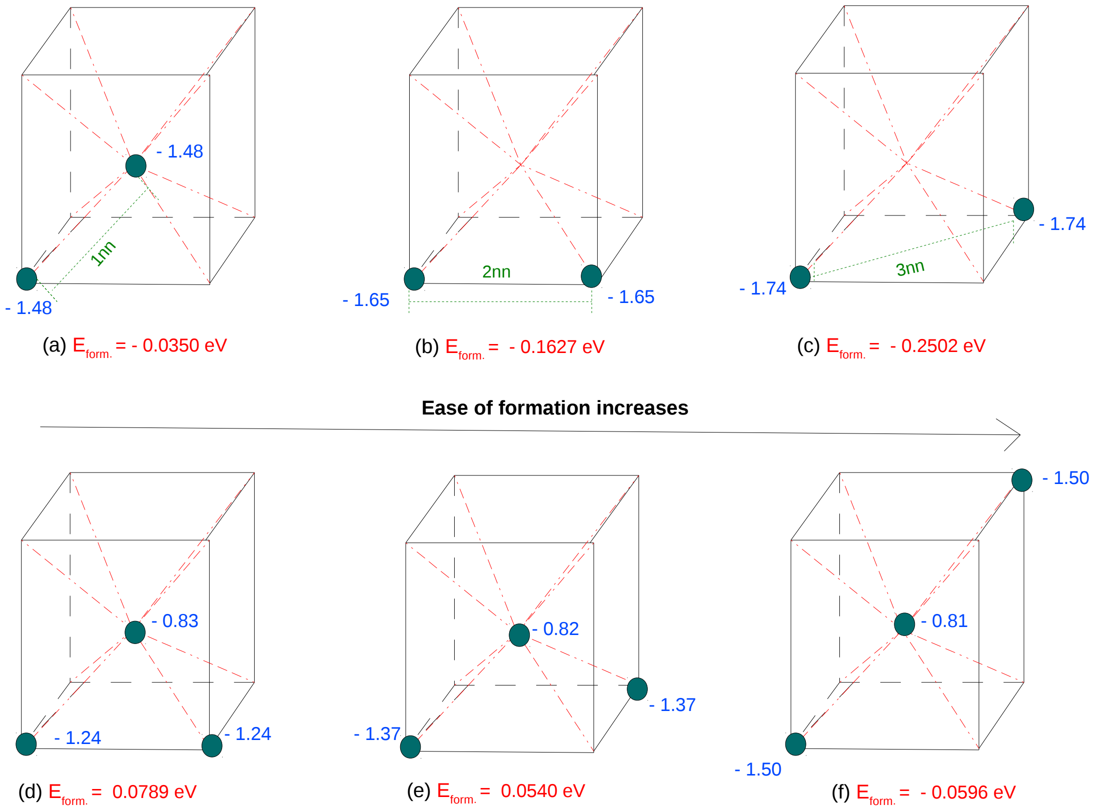

(a) $E_{form.}$ = - 0.0350 eV

(b) $E_{form.}$ = - 0.1627 eV

(c) $E_{form.}$ = - 0.2502 eV

(d) $E_{form.}$ = 0.0789 eV

(e) $E_{form.}$ = 0.0540 eV

(f) $E_{form.}$ = - 0.0596 eV

Figure 4.3: Two and three Cr substitutions in bcc Fe
Ease of formation increases as well as the Cr atoms are taken farther away.

make appropriate predictions of the microstructural evolution. However, when approached through experiments these point defect calculations have proved problematic, and at times even inaccessible. Vacancy migration energy in bcc Fe is one such famous example of witnessing a wide a spread in experimental results. Though, the ratio of vacancies to atomic sites in a crystal is usually not more than $10^{-4} - 10^{-3}$ (for temperatures below the melting point); it is these defects (and interstitials) which cause the kinetics of the system leading to material's key responses.

The formation energy of a monovacancy of N atoms by:

$$E^{vac}_{form} = E_{(N-1,1)} - \frac{N-1}{N} E_{(N,0)} \tag{4.3}$$

where it is assumed that the supercell size has not been affected significantly due to the formed vacancy. My reults of the vacancy formation energy for bcc Fe is 2.11 eV, are in good agreement with reported ab initio values of 2.02 - 2.15 eV [12, 13, 14]. The atoms surrounding the monovacancy isotropically relax towards or away with respect to the the vacancy. Figure 4.4 explains the trend of relaxation of atoms for 1nn-4nn neighbours of the vacancy.[1] It showed a typical trend seen in bcc transition metals of an alternative inward and outward relaxations near the vacancy. The magnitude of these relaxations decrease monotonically with increase in distance from the vacancy as the strain field due to vacancies falls off with distance. The magnetic moments on relevant atoms is represented in blue colour (in the units of bohr magnetons). The magnitude of relaxations and the observed trend are in concurrence with the reported values[12, 20].

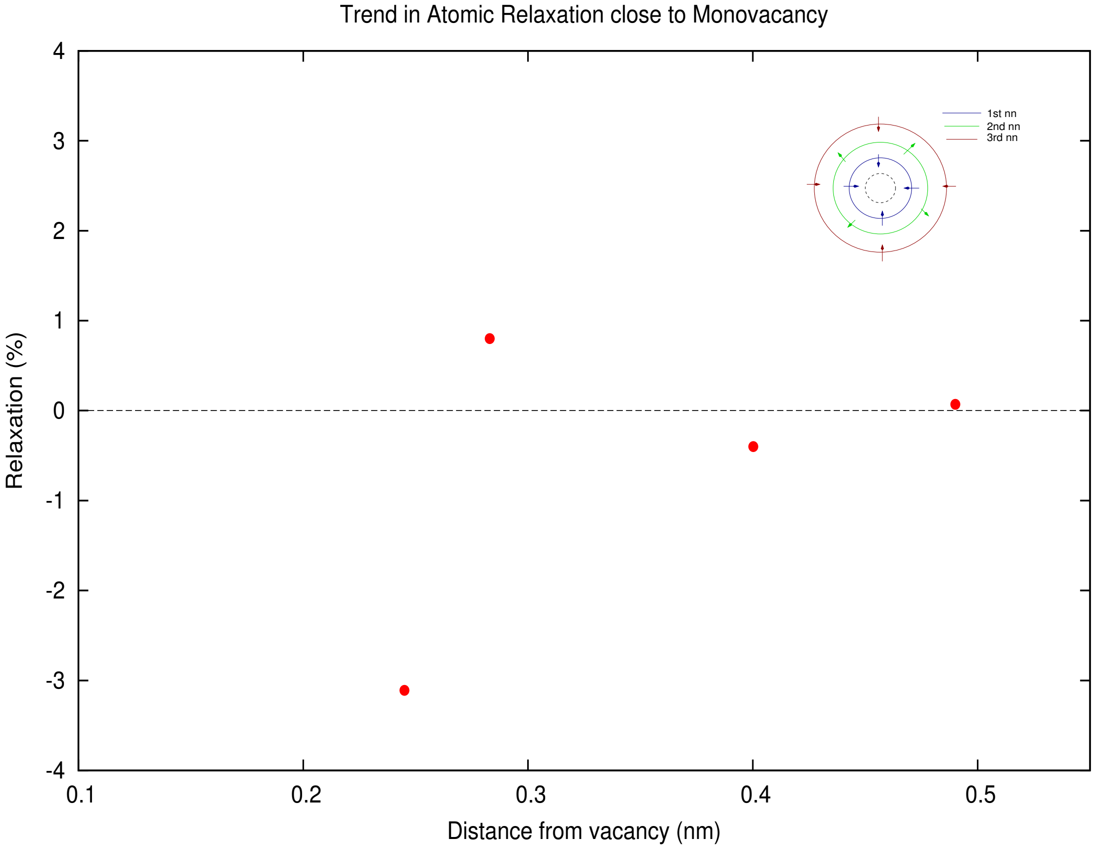

Figure 4.4: Relaxation of vacancy neighbours in bcc 127-atom Fe
A pattern common in bcc transition metals

[1] It should be noted that the figure of crystal structures are not of the entire supercell (of 128-atoms). They depict only the primitive cell of 2-atoms (within the supercell of 128-atoms) containing the defects. Also, interaction of defects located in different primitive cells of the supercell have not been covered in this study.

4.2.1 NEB Results of Vacancy Migration in bcc Fe and Cr

These DFT optimized configurations are used for calculating the possible migration barriers for a reaction pathway. For the simplest case, the migration barrier for a vacancy to move to a first nearest neighbour site (1nn) in bcc Fe is found to be 0.69 eV. The reported ab initio values are in the range 0.65 - 0.75 eV. However, as mentioned in [12], the experimental value for this migration has been controversial and range over a wide range of 0.55 - 1.28 eV. This spread is attributed to the difficult task in obtaining Fe crystals without impurities, which directly affect the diffusivity of the vacancies by trapping them. The experimental results of [22] reported this barrier to be 0.55 eV using high-purity crystals, which is relatively closest to the range of ab-initio predictions. The observed barrier for 1nn vacancy migration in bcc Cr is 0.79 eV, while the experimental value is 0.88 eV. This high barrier should be seen with the fact that Cr is known to be the least diffusive for monovacancies with highest migration barrier among all bcc transition metal crystals[23].

4.3 Vacancy and Solute Cr Substitution in bcc Fe

Cr-Vacancy binding energy is found to be 0.055 eV, consistent with reported ab initio value [14] and an experimental study [21]using muon spectroscopy, where it was predicted that Cr-Vacancy binding energy to be less than 105 meV. This result indicates a low tendency of vacancy and Cr to remain bound to each other, and hence such an interaction could be neglected while considering other dominant interactions. Table 4.2 gives the formation energy of Vac-Cr configurations for 1-4nn positions. We can observe that spread of values is not very significant and there is no clear definite trend in the formation energies with varying Cr-Vac distances.

In the case of 2nn Cr-Vac configuration, a possibility of 2nn migration by Cr was also examined. The barrier of such a big jump (5% greater in terms of distance) is found to be as big as 2.27 eV. From figure 4.5 it could be observed that this value is greater by 1 eV than the sum of any two unit migrations. Hence, hereafter only unit migrations of 1nn jumps have been considered.

With an increase in species of defects in a system, the possibilities of migrations also increases. In a single vacancy and Cr substitutional defect, it is observed that Cr is more probable to diffuse to a nearby vacancy (than the matrix atoms), owing to migration barrier about 0.23 eV lower than that of nearby Fe, as depicted in figure4.6. Also, by observing the blue, black, and red lines in 4.6, the Fe migration to a nearest neighbour site remains unaffected by relative position of Cr, and is also same as the case of pure bcc Fe. This behaviour is also observed in the magnetic moments of the interacting atoms. Comparing substituted Cr in bcc Fe and pure bcc Cr, Cr becomes antiferromagnetically coupled to the Fe environment in the former case, whereas its nonmagnetic in pure crystal form. However, the Fe atoms nearby the substituted Cr, do not exhibit any change in their local magnetic moment; thus indicating no considerable change due to the presence of Cr at 2nn and 3nn positions.

Table 4.2: Formation energies in 1substituted Cr and 1 vacancy configurations in bcc Fe

Cr-Vac distances	My Results	Olsson *et al.*[14]
1nn	1.92	1.98
2nn	1.96	2.02
3nn	1.97	—
4nn	1.94	—

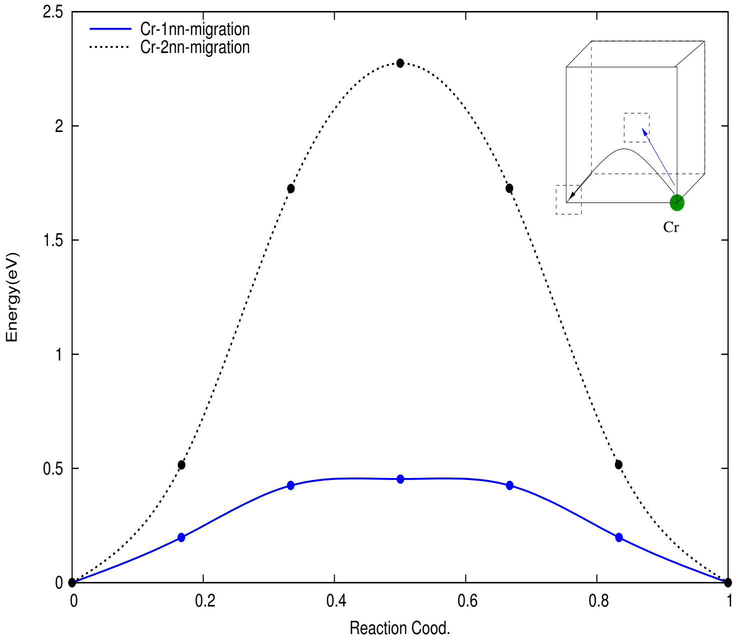

Figure 4.5: Second nearest neighbour jump by Cr in bcc 127 Fe atoms
Big 2nn jump for Cr has a rare possibility in comparison to two back-to-back 1nn unit processes

4.3.1 Adding Substitutional Cr Atoms

The structural and NEB calculations were performed by adding an additional Cr substitution. Figure 4.7 offers two cases where Cr-vacancy interaction has

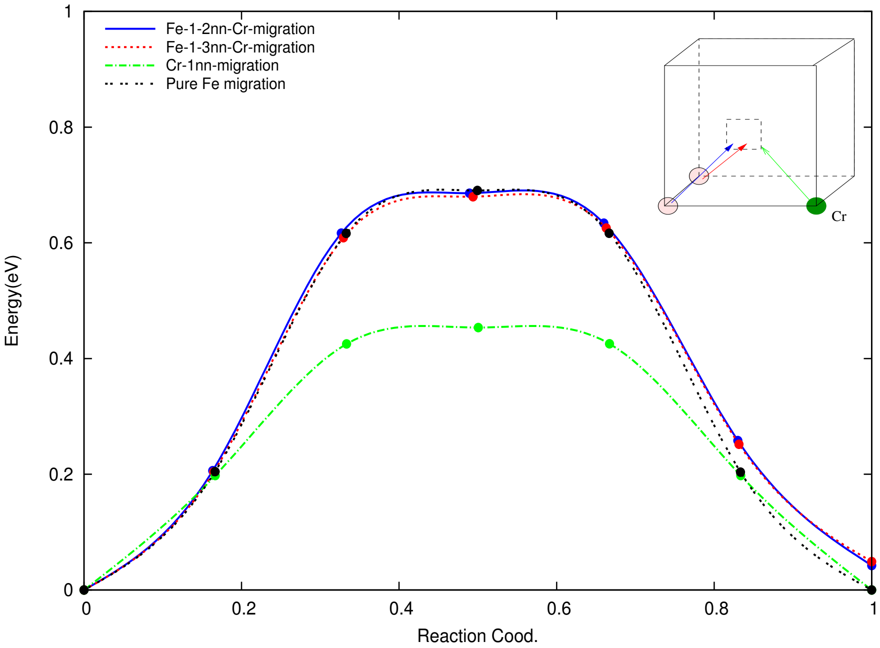

Figure 4.6: Configurations with 1Cr and 1 vacancy in 126 bcc Fe The barrier for Fe migration remains the same irrespective of position of Cr, while Cr's diffusivity increases trenedously in comparison to pure bcc Cr

been nomalized in (a, b, c), and where Cr-Cr interaction have been normalized in (d, e, f). Clearly, (a, b, c) have a definite trend of decreasing formation energy with increasing Cr-Cr distance, as earlier discussed in section 4.1.2. This reinstates the important role played by Cr-Cr interaction in deciding the energetics of these configurations. Whereas, in (d, e, f) there appears a lack of a clear trend as the differentiating interaction is the one with the vacacny-Cr which is understood to not have any substantial effect. In considering the NEB results, figure 4.8 uses the notation of figure 4.7.

Clearly, $\Delta E_{ad} < \Delta E_{be} < \Delta E_{cf}$, where, ΔE is the difference of energy between reactants and products.

Also, $E(TS)_{ad} > E(TS)_{be} > E(TS)_{cf}$, where, $E(TS)$ represents the energy of the transition state of the corresponding migration.

Further, $E(TS)_{cf} = E(TS)_{singleCr}$

This implies that Cr-Cr inteaction falls off after 4nn distance. These trends can be explained by strong Cr-Cr repulsive interaction (dominating the Cr-Vacancy interaction) in these low Cr concentration regime. Similar trend is seen for the magnetic moment.

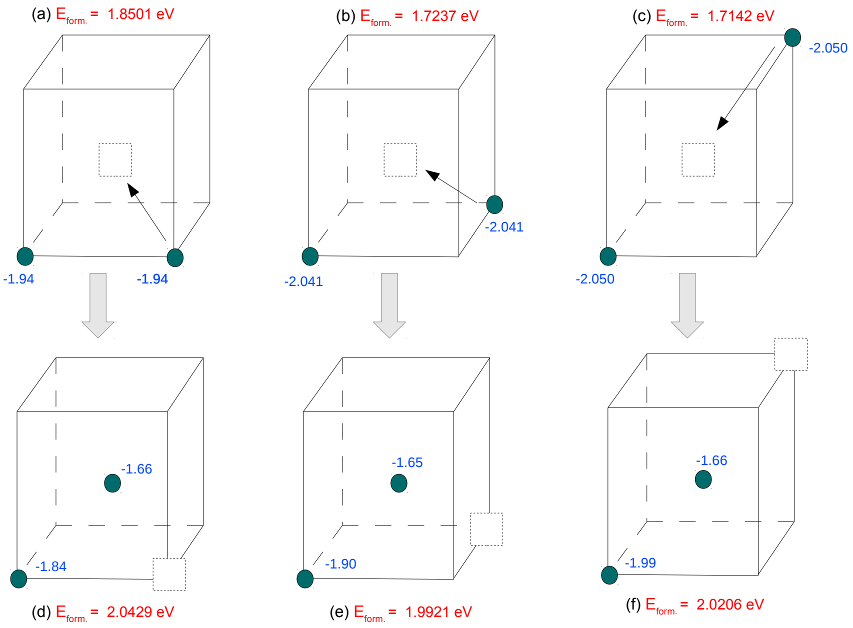
(a) $E_{form.}$ = 1.8501 eV
(b) $E_{form.}$ = 1.7237 eV
(c) $E_{form.}$ = 1.7142 eV
-1.94
-1.94
-2.041
-2.041
-2.050
-2.050
-1.66
-1.84
-1.65
-1.90
-1.66
-1.99
(d) $E_{form.}$ = 2.0429 eV
(e) $E_{form.}$ = 1.9921 eV
(f) $E_{form.}$ = 2.0206 eV

Figure 4.7: Configuratons with 2 Cr and 1 vacancy in 125 bcc Fe:

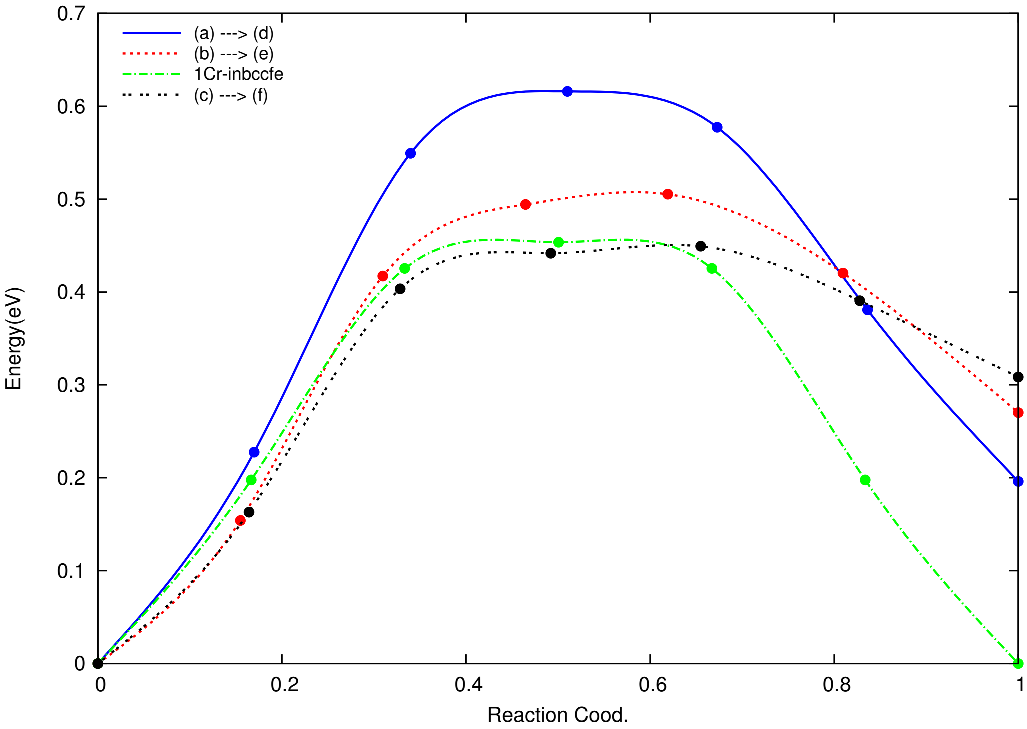

Figure 4.8: Migration barriers for different 2Cr-1Vac configurations in 125 Fe atoms are pictured in figure 4.7

Cr-Cr interaction clearly dominates, but falls off by the 4nn distance

4.4 KMC Simulation: Vacancy Diffusion

These DFT and NEB results have been utilized by my KMC code to setup a simulation platform for a kinetic study of the defects. Until now, a code for simulating the vacancy diffusion for bcc geometries is completed and tested. This was verified in two cases:
1. Vacancies + bcc Fe system
2. Vacancies + 50% Cr + 50% Fe in bcc geometry

We use the following models for calculating the diffusivities of vacancies in our system:

- Coefficients of diffusion is given by [24]

  $$D_{\text{vac}} = a^2 \mathrm{C}_{\text{vac}} \nu f_{\text{vac}} \exp(-\frac{E_{mig}}{k_b T}) \tag{4.4}$$

  where, a is the jump distance, C_{vac} is the concentration of vacancy, f_{vac} is the correlation factor of the vacancy ν is prefactor calculated in HTST and E_{mig} is the migration energy barrier of vacancy in the environment considered. By writing all the constants together as D_o the equation can be written as:

  $$D = D_o \exp(-\tfrac{E_{mig}}{k_b T})$$

  $$\implies ln(D) = -\frac{E_{mig}}{k_b T} + ln(D_o) \tag{4.5}$$

  where, it is seen that graph of $ln(D)$ v/s $\frac{1}{T}$ is linear with slope $-\frac{E_{mig}}{k_b}$

- Relation for coefficient of diffusion given by Einstein, as a random walk problem in a limiting case (in 3-dimension)[27] is:

  $$D = \frac{< \Delta r^2(t) >}{6t} \tag{4.6}$$

  where, $< \Delta r^2(t) >$ is the mean squared displacement of the diffusing entity, and t is the kmc simulated time[2]

[2] This is the simplest form of the equation for Diffusion constant for a limiting case of a random walk. However, as described in [28], a more refined form of the same is: $D = \frac{zC\nu<\Delta r^2>f}{6}$, where z is number of possible sites where the vacancy can migrate, C is the concentration of vacancies, and f is the correlation factor for vacancy in the considered geometry.

4.4.1 Vacancy in bcc Fe

The vacancy diffusion migration barrier in bcc Fe is found to be 0.69 eV using NEB, as reported in 4.2. Using this, kmc simulations were performed in the temperature range of 300-1500 K, with systems of 20 thousand and 8 thousand atoms. After feeding this migration barrier, the simulation ran for 10^6 steps and then, $< \Delta r^2(t) >$ was calculated over the simulated time. These were used to calculate D using 4.6. As mentioned in 4.5, by plotting ln(D) versus $\frac{1}{T}$ we can derive E_{mig}(as k_b is constant), which in fact was our input parameter.

$\Longrightarrow$ Hence, one of the ways to verify the code could be to check whether the input and output barriers match to the desired accuracy. The results are reported in Table 4.3. Also, the linear curve for ln(D) versus $\frac{1}{T}$ has been shown for 20 thousand atom system in 4.9.

Table 4.3: Input and Output migration energies for vacancy diffusion in bcc Fe:

Atoms	20x10^3 10^{-1}% vac	20x10^3 10^{-2}% vac	8x10^3 10^{-1}% vac
Input E_{mig}(eV)	0.69	0.69	0.69
Output E_{mig}(eV)	0.69001	0.68993	0.69005

4.4.2 Vacancy diffusion in bcc Fe and Cr system

After witnessing that Cr has a considerable lower migration barrier (0.23 eV) than Fe atoms, as reported in 4.3, we simulated a system of 50% bcc Fe and 50%Cr atoms. This concentration gave them an equal chance of migrating to the vacancy site, but the kinetics was constrained by their respective migration barrier; and thus,constraining their respective diffusivities. The ratio of calculated value of diffusion constants through the simulation using 4.6 is as follows:

$$\frac{D_{Cr}}{D_{Fe}} = 8.6 \text{ x } 10^3, \qquad exp(\frac{E_{Fe} - E_{Cr}}{k_b T}) = 9.1 \text{ x } 10^3$$

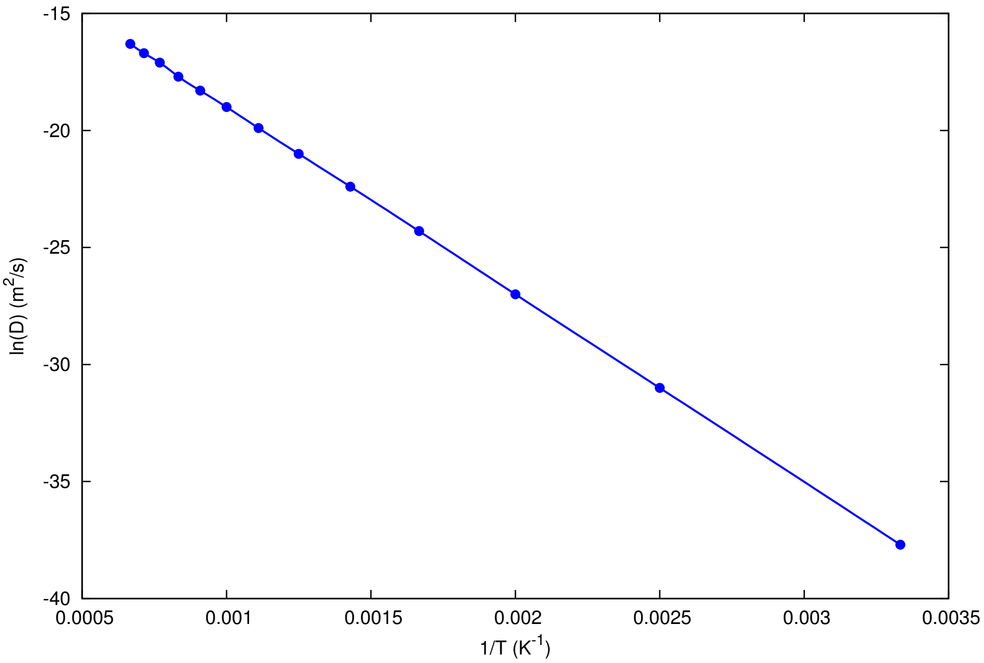

Figure 4.9: 20 thousand atoms with 0.1% vacancies for temperature range 300-1500 K
The slope of the graph gives E_{mig} to be 0.69001 eV, as reported in table 4.3

The exponential term represents probabilistically expected order of difference in the diffusivities by considering 4.4. Hence, it can be seen that the simulated results are in reasonable agreement with the probabilistically predicted order of difference in the diffusivities in Fe and Cr; and, it is concluded that at 400 K Cr migrates about 10^3 times more than Fe when present in equal concentration in the alloy.

4.5 Conclusions

In this work, we have successfully modeled bcc Fe-Cr alloys over large scales of length and time, from DFT electronic structure calculations up to diffusional transport of vacancies. Adding interstitials and possible migrations for other significant environments in these systems could help us better understand the real kinetics of these alloys. Further, inferences drawn by comparing broad trends of migration barriers for different environments could significantly reduce the migration possibilities to be examined. As the migrations get sophisticated the KMC code would need to be further worked upon to accommodate them, to appropriately model the kinetics of the alloy.

Appendix A

A.1 Proof: First HK Theorem, described in Sec. 2.2

Proof by Contradiction:
Consider two non-degenerate ground states Ψ_1 and Ψ_2 of N-electron system in two distinct external potentials $v_1(\mathbf{r})$ and $v_2(\mathbf{r})$.
Assumption (to be contradicted): Two systems can still have the same electronic ground state densities as; say n($\mathbf{r}$)
$\mathcal{H}_1 = K.E + P.E + \sum\limits_{i=1}^{N} v_1(\mathbf{r}_i)$
$\mathcal{H}_2 = K.E + P.E + \sum\limits_{i=1}^{N} v_2(\mathbf{r}_i)$

As Ψ_1 and Ψ_2 are the ground states of the two systems they satisfy the Schrodinger Equations:
$\mathcal{H}_1\Psi_1 = E_1\Psi_1, \qquad (1)$
$\mathcal{H}_2\Psi_2 = E_2\Psi_2, \qquad (2)$

By the Rayleigh-Reitz principle in quantum mechanics we can write from (1) and (2): $\langle\Psi_1|\mathcal{H}_1|\Psi_1\rangle < \langle\Psi_2|\mathcal{H}_1|\Psi_2\rangle$

$\Rightarrow E_1 < \langle\Psi_2|\mathcal{H}_1|\Psi_2\rangle$

$\Rightarrow E_1 < E_2 + \langle\Psi_2|\ v_1((\mathbf{r}) - v_2(\mathbf{r})\ |\Psi_2\rangle$

$\Rightarrow E_1 < E_2 + \int n(\mathbf{r})[v_1((\mathbf{r}) - v_2(\mathbf{r})]\,\mathrm{d}\mathbf{r} \qquad [\mathbf{1}]$
Similarly, as the two ground states Ψ_1 and Ψ_2 have the same charge densities n($\mathbf{r}$) we can write:

$\Rightarrow E_2 < E_1 + \int n(\mathbf{r})[v_2((\mathbf{r}) - v_1(\mathbf{r})]\,\mathrm{d}\mathbf{r} \qquad [\mathbf{2}]$

Adding [**1**] and [**2**]

$\Rightarrow E_1 + E_2 < E_2 + E_1 \Rightarrow$ A clear contradiction.

Hence, our basic assumption of same ground-state densities for two distinct potentials has to be false. It is thus proved that the ground state electron density is uniquely defined by the external potential and vice-versa.

A.2 My KMC code in C

```
//1.) Read from the INPUT.dat

//2.)Decide and Create the geometry --> text file (Structure.dat)

//3.) (Structure.dat) text file --> an array (Data)

//4.) First nearest neighbour coordinates for all: from Data ---> FNN.dat --> fnncood (array)

//5.) Incorporating periodic boundary conditions in fnncood (array) --> FNNnew.dat

//6.) Getting respective indices of first nearset neighbours: fnncood --> FNNind.dat

//7.) Creating an array of indices of first nearest neighbours of all atoms: FNNind.dat --> FULLfnn (array)

//8.) Deciding the percentage of Vacancies and randomly creating them:vacind and vaccood ---> Vacancy.dat

//9.) File for fnn for vacancies: FULLfnn (array) --> FNNvac.dat

//10.) Event flile from: vacind + FNNvac.dat --> Event

//.............................................................................................
#include <math.h>         //use -lm while compiling!!!
#include <stdio.h>
#include <stdlib.h>
#include <time.h>

//Translate INPUT.dat --> IN[8]
main()
{
float IN[10];
FILE* file = fopen ("INPUT2.dat", "r");
if (file == NULL)
    { printf("\n CanâĂŹt open %s\n","INPUT.dat");
        exit;
    }
int h;
for(h= 0; h < 10; h++)
  {
        fscanf(file,"%f", &IN[h]);
  }
  fclose (file);
float Lconst = IN[7];

//Decides and creates Structure.dat
int atoms;
float ux,uy,uz;
ux=IN[0];
uy=IN[1];
uz=IN[2];
printf("\nThe cell sought is of SIZE %f %f %f units\n",ux, uy, uz);
atoms=2*(ux*uy*uz);
printf("\nNumber of atoms in the BCC configuration is: %d \n", atoms);
FILE *fp=fopen("Structure.dat", "w");
if (fp == NULL)
    { printf("\n CanâĂŹt open %s\n","text");
        exit;
    }
float a, b, c, i, j, k;
for (i=0; i<=(ux -1); i++)
{
        for (j=0; j<=(uy -1); j++)
        {
                for (k=0; k<=(uz -1); k++)
                {
                  fprintf(fp, "%f %f %f\n",i, j, k);
                 }
        }
}
for (a=0.5; a<=(ux -0.5); a++)
{
        for (b=0.5; b<=(uy -0.5); b++)
        {
                for (c=0.5; c<=(uz -0.5); c++)
                {
                  fprintf(fp, "%f %f %f\n", a, b, c);
                 }
        }
}
fclose(fp);


//Translating Structure.dat --> Data[atoms][3]
float Data [atoms][3];
int l, m, n;
fp=fopen("Structure.dat", "r");
```

```
if (fp == NULL)
    { printf("\n CanâĂŹt open %s\n","Structure.dat");
      exit;
    }
for(l = 0; l < atoms; l++)
  {
    for (m=0; m< 3; m++)
      {
        fscanf(fp, "%f", &Data[l][m]);
      }
   }
fclose(fp);


//Translate Data --> first draft of FNNcood.dat (without PBC)
FILE *fp1= fopen("FNNcood.dat", "w");
if (fp1 == NULL)

    {
        printf("\n CanâĂŹt open %s\n","FNNcood.dat");
        exit;
    }

for (l=0; l<atoms; l++)
{
        for (i=-0.5; i<1.0; i++)
        {
                for (j=-0.5; j<1.0; j++)
                {
                        for (k=-0.5; k<1.0; k++)
                        {
                           fprintf(fp1, "%f\t %f\t %f \n", Data[l][0]+i, Data[l][1]+j, Data[l][2]+k);

                        }
                }
        }
}
fclose (fp1);


//Translate FNN.dat --> 1st draft of fnncood[atoms*8][3] (without PBC)
float fnncood[atoms*8][3];
fp1=fopen("FNNcood.dat", "r");
if (fp1 == NULL)

    {
        printf("\n CanâĂŹt open %s\n","FNNcood.dat");
        exit;
    }
for(l = 0; l < (atoms*8); l++)
  {
    for (m=0; m< 3; m++)
      {
        fscanf(fp1, "%f", &fnncood[l][m]);
      }
   }

fclose(fp1);


//Introducing PBC in fnncood[atoms*8][3]
for( l = 0; l < atoms*8; l++)
{
 for( m = 0; m < 3; m++)
   {
        if (fnncood[l][m] < 0.0)
        {
          if (m==0)
                {
                  fnncood[l][m]= ux + fnncood[l][m];
                }
          else if (m==1)
                {
                  fnncood[l][m]= uy + fnncood[l][m];
                }
          else if (m==2)
                {
                  fnncood[l][m]= uz + fnncood[l][m];
                }
        }
        else if ((fnncood[l][m] > (ux-0.5)) && (m==0))
                {
                   fnncood[l][m]= fnncood[l][m] - ux;
                }
        else if ((fnncood[l][m] > (uy-0.5)) && (m==1))
                {
                  fnncood[l][m]= fnncood[l][m] - uy;
                }
        else if ((fnncood[l][m] > (uz-0.5)) && (m==2))
                {
                  fnncood[l][m]= fnncood[l][m] - uz;
                }
    }
}
```

```
//Translate fnncood[atoms*8][3] --> FNNcoodNEW.dat (having PBC)
FILE *fp4=fopen("FNNcoodNEW.dat", "w");
if (fp4 == NULL)
    {
        printf("\n CanâĂŹt open %s\n","FNNnew.dat");
        exit;
    }
for( l = 0; l < atoms*8; l++)
{
    for( m = 0; m < 3; m++)
   {
        fprintf(fp4, "%f\t", fnncood[l][m]);
   }
fprintf(fp4, "\n");
}
fclose (fp4);



//Translate fnncood array --> FNNind.dat
FILE *fp3=fopen("FNNind.dat", "w");
if (fp3 == NULL)
    { printf("\n CanâĂŹt open %s\n","FNNind.dat");
      exit;
    }
int fnnind;
float numf, num;
int numi,r,s;
for(r=0; r < atoms*8; r++)
  {
         num=fnncood[r][0];
         numi=num;
         numf=numi;
         if (numf==num)      //Condition to be in upper matrix
          {
                    fnnind= uz*uy*fnncood[r][0] + uz*fnncood[r][1] + fnncood[r][2] + 1;
                    fprintf(fp3, "%d\t", fnnind);
                    if ((r+1)%8 == 0)
                    fprintf(fp3,"\n");
          }
        else       //Condition to be in lower matrix
          {
                    s=fnncood[r][0];
                    m=fnncood[r][1];
                    n=fnncood[r][2];
                    fnnind=uz*uy*s + uz*m + n + 1+ (atoms)/2;
                    fprintf(fp3, "%d\t", fnnind);
                    if ((r+1)%8 ==0)
                    fprintf(fp3,"\n");
          }
 }
fclose(fp3);


//Translate FNNind.dat --> COMPLETE FNN IDEA IN FULLfnn[atoms][10]
fp3=fopen("FNNind.dat","r");
if (fp3 == NULL)
    { printf("\n CanâĂŹt open %s\n","FNNind.dat");
      exit;
    }
int FULLfnn[atoms][10];
for(l = 0; l < atoms; l++)
  {
    for (m=1; m<9; m++)
      {
        fscanf(fp3, "%d", &FULLfnn[l][m]);
      }
    FULLfnn[l][0]=l+1;         //aTOM iNDEX Number
    FULLfnn[l][9]=1;       //All are atomic sites
   }
fclose(fp3);


//Decide perercentage, number of Vacancies
float nvac0, per;
int nvac;
per=IN[3];
printf("\nPercentage of Vacancies desired: %f\n", per);
nvac0= atoms*(per/100.0);
nvac=round(nvac0);
printf("\nNumber of Vacancies: %d\n", nvac);


//nvac --> Randomly generated number 0-1, rno[nvac]
double rno[nvac];
srand (time (NULL) );
for (l=0; l<nvac; l++)
{
rno[l] = (double)rand()/(double)RAND_MAX;
}

```

```

//rno[nvac] --> Indices and Coordinates of Vacancies, vacind[nvac], vacood[nvac][3]
int vacind[nvac];
float vaccood[nvac][3];
for (l=0; l<nvac; l++)
{
        vacind[l]=atoms*rno[l];
        while (vacind[l]==0)
        {
                        vacind[l]=((double)rand()/(double)RAND_MAX)*atoms;
        }
}




//: HOW TO MAKE A SET OUT OF AN ARRAY (not reducing the total no. of elements)
for (l=0; l<nvac; l++)
{
        for (m=l+1; m<nvac;m++)
        {
                while ((vacind[m]==vacind[l])||(vacind[m]==0))//Removing repetitive elements from vacin
                {
                        vacind[m]=((double)rand()/(double)RAND_MAX)*atoms;
                }
        }
       FULLfnn[(vacind[l])-1][9]=0;
}

FULLfnn[(vacind[nvac-1] -1)][9]=0; //separately making the last vacancy index to zero

printf("Vacancy Indices:\n");
for (l=0; l<nvac; l++)
{
printf("%d\n", vacind[l]);
}




//Percentage of Cr in Fe-Cr alloy
float ncr0, percr;
int ncr;
percr=IN[8];
printf("\nPercentage of Cr desired: %f\n", percr);
ncr0= atoms*(percr/100.0);
ncr=round(ncr0);
```

```
printf("\nNumber of Cr: %d\n", ncr);

//nvac --> Randomly generated number 0-1, rno[nvac]
double rnocr[ncr];
for (l=0; l<ncr; l++)
{
rnocr[l] = (double)rand()/(double)RAND_MAX;
}


//rno[nvac] --> Indices and Coordinates of Vacancies, vacind[nvac], vacood[nvac][3]
int crind[ncr];
float crcood[ncr][3];
for (l=0; l<ncr; l++)
{
        crind[l]=atoms*rnocr[l];
        while (crind[l]==0)
        {
                        crind[l]=((double)rand()/(double)RAND_MAX)*atoms;
        }
}



//: HOW TO MAKE A SET OUT OF AN ARRAY (not reducing the total no. of elements)
for (l=0; l<ncr; l++)
{
        for (m=l+1; m<ncr;m++)
        {
             for (n=0; n<nvac; n++)
              {
                while ((crind[m]==crind[l])||(crind[m]==0)||(crind[m]==vacind[n]))//Removing repetitive
                {
                        crind[m]=((double)rand()/(double)RAND_MAX)*atoms;
                }
              }
        }
       FULLfnn[(crind[l])-1][9]=-1;
}

FULLfnn[(crind[ncr-1] -1)][9]=-1; //separately making the last vacancy index to zero



printf("Cr Indices:\n");
for (l=0; l<ncr; l++)
{
```

```
printf("%d\n", crind[l]);
}

/*
//Translate vacind[nvac] --> vacood[nvac][3]
for (l=0; l<nvac; l++)
{
        for(m=0; m<3; m++)
        {
                vaccood[l][m] = Data[(vacind[l]-1)][m];
        }
}
*/


/*COMPLETE IDEA OF A CONFIGURATION IN PRINTING FULLfnn
printf("\nFULL First Nearsest Neighbours of all the lattice sites:\n");
printf("CONFIGURATION 1\n\n");
for(l = 0; l < atoms; l++)      //printing FULLfnn
  {
    for (m=0; m< 10; m++)
        {
          printf("%d\t", FULLfnn[l][m]);
        }
    printf("\n");
  }

/*Generating "Reduced Data" with [Reduced Data]= [Data][H inverse]

float ReducedData[atoms][3];
float H[3][3]={

                     {Lconst/2, Lconst/2, -Lconst/2},
                     {-Lconst/2, Lconst/2, Lconst/2},
                     {Lconst/2, -Lconst/2, Lconst/2}
              };



float determinant=0;
for(l=0;l<3;l++)
      determinant = determinant + (H[0][l]*(H[1][(l+1)%3]*H[2][(l+2)%3] - H[1][(l+2)%3]*H[2][(l+1)%3

   printf("\nInverse of matrix is: \n\n");
   for(l=0;l<3;l++){
      for(m=0;m<3;m++)
           printf("%.2f\t",((H[(l+1)%3][(m+1)%3] * H[(l+2)%3][(m+2)%3]) - (H[(l+1)%3][(m+2)%3]*
       printf("\n");
   }

float Hinv[3][3];
for (l = 0; l < atoms; l++)
{
  for (m=0; m< 3; m++)
  {
     ReducedData[l][m]= Data[l][0]*Hinv[0][m] + Data[l][1]*Hinv[1][m] + Data[l][2]*Hinv[2][m];
  }
}
//Reduced cood should belong to [0,1). Hence using "floor function(gif)"
 for(l = 0; l < atoms; l++)
    {
        for (m=0; m< 3; m++)
         {
            if (ReducedData[l][m]>=1.0)
            {
               ReducedData[l][m]=ReducedData[l][m]-floor(ReducedData[l][m]);
            }
         }
    }

float Data1[atoms][3];
for(l=0; l<atoms; l++)
{
  for (m=0; m<3; m++)
  {
    Data1[l][m]=Data[l][m];
  }

  if (FULLfnn[l][9]==0)
   {
    Data1[l][0]=-1.0;
   }
}

FILE* fp5;
    fp5 = fopen("config1.dat","w");
if (fp5 == NULL)
    { printf("\n CanâĂŹt open %s\n","config1.dat");
      exit;
    }
for(l = 0; l < atoms; l++)
    {
      if (Data1[l][0]==-1.0)
           {
             fprintf(fp5, "%f %s ", 29.0, "Cu");
           }

       else
           {
              fprintf(fp5, "%f %s ", 26.0, "Fe");
           }

       for (m=0; m< 3; m++)
         {
           fprintf(fp5, "%f ", ReducedData[l][m]);
         }
    fprintf(fp5, "%d %d %d", 0, 0, 0);
    fprintf(fp5, "\n");
   }

fclose(fp5);
*/

//DECLARING A DYNAMIC EVENT TABLE................................
float **Event;
Event = (float**)malloc((nvac*8)*sizeof(float *));
if(Event == NULL)
                {
                 printf("out of memory 1st time\n");
                 return;
                }
for(l = 0; l < nvac*8; l++)
                {
                 Event[l] = (float*)malloc(5*sizeof(float));
                 if(Event[l] == NULL)
                        {
                        printf("out of memory 2nd time\n");
                        return;
                        }
                }


//Begin KMC:......................................................
int nEvent;
int Temp;
Temp=IN[6];
double Kb= 8.6173*pow(10,-5); //in eVâĂĹK^âĹŠ1 since the barriers are in eV
int step, kmcsteps=IN[5];
long double time=0.0, timeTE, timecr=0.0;
float R, R1;
int TheEvent;
int na, nv;
float DataConfig[atoms][3];
char OutputConfig[20], Cu, Fe;
FILE* fp6;
float SDstep, SD=0.0;
float xo, yo, zo;
float SDstepcr, SDcr=0.0;

FILE* msdp = fopen("msd_vs_time.dat", "w");
if (msdp == NULL)
    {
        printf("\n CanâĂŹt open %s\n","msd_vs_time.dat");
        exit;
    }

FILE* msdpcr = fopen("msdcr_vs_time.dat", "w");
if (msdpcr == NULL)
    {
        printf("\n CanâĂŹt open %s\n","msdcr_vs_time.dat");
        exit;
    }
//****THE KMC LOOP*****
for (step=1; step <= kmcsteps; step++)
{

nEvent=0;

/*
for(l=0; l<atoms; l++)
{
  for (m=0; m<3; m++)
  {
    DataConfig[l][m]=Data[l][m];
  }

  if (FULLfnn[l][9]==0)
   {
    DataConfig[l][0]=-1.0;
   }
}

fp6 = fopen(OutputConfig,"w");
if(fp6 == NULL)
                {
                 printf("out of memory 3rd time\n");
                 exit;
                 }
    sprintf(OutputConfig,"config%d.dat", step+1);


for(l = 0; l < atoms; l++)
    {
       if (DataConfig[l][0]==-1.0)
           {
             fprintf(fp6, "%f %s ", 29.0, "Cu");
           }

       else
           {
              fprintf(fp6, "%f %s ", 26.0, "Fe");
           }

       for (m=0; m< 3; m++)
         {
           fprintf(fp6, "%f ", ReducedData[l][m]);
         }
     fprintf(fp6, "%d %d %d", 0, 0, 0);
     fprintf(fp6, "\n");
    }
fclose(fp6); */
//Making Event Table
for (l=0; l< atoms; l++)
{
  if (FULLfnn[l][9]==0)
  {
       for (m=1; m<9; m++)
        {
          if (FULLfnn[(FULLfnn[l][m] -1)][9] != 0)
           {
                Event[nEvent][0]=nEvent+1;
                Event[nEvent][1]=FULLfnn[l][0];
                    if (FULLfnn[(FULLfnn[l][m] -1)][9] == -1)
                   {
                        Event[nEvent][3]=IN[9];
                        Event[nEvent][4]=pow(10, 13)*exp(-IN[9]/(Kb*Temp));
                   }

                    else if (FULLfnn[(FULLfnn[l][m] -1)][9] == 1)
                   {
                     Event[nEvent][3]=IN[4];
                     Event[nEvent][4]=pow(10, 13)*exp(-IN[4]/(Kb*Temp));
                   }
                Event[nEvent][2]=FULLfnn[l][m];
                nEvent=nEvent+1;
           }
        }
  }
}
printf("\nTotal Number of Events for Configuration %d are: %d\n", step, nEvent);
printf("\nThe Events table is as follows:\n");
/*for (l=0; l<nEvent; l++)
{
        for (m=0; m<5; m++)
        {
          printf("%lf\t", Event[l][m]);
        }
        printf("\n");
}*/

float Sumk[nEvent];
//Array for every n such that Sum(n) = k1+k2+....kn, Sum[nEvent]
//printf("\nThe SumK array:\n");
for(l=0; l< nEvent; l++)
{
        float sum=0.0;
        for (n=0;n<=l;n++)
        {
         sum= sum + Event[n][4];
        }
  Sumk[l]=sum;
// printf("%f\n",Sumk[l]);
}


//Generate the KMC Random Number between 0-1
R=(double)rand()/(double)RAND_MAX;
printf("\nRandom number Of KMC: %f\n", R);
printf("SUMKTOTAL %f\n", Sumk[nEvent - 1]);
printf("Random Number*SUMKtotal for KMC is %f\n", R*Sumk[nEvent -1]);


//EVENT SELECTION CRITERION: Get the TheEvent such that: k(i) > RandomNumber*SUMKtotal > k(i-1)
for(l=0; l< nEvent; l++)
{
if ((R*Sumk[nEvent - 1])<Sumk[l])
break;
}
//TheEvent is the index number
R1=(double)rand()/(double)RAND_MAX;
TheEvent=l+1;
```

```
timeTE=(-1*log(R1)/(Sumk[nEvent - 1]));
printf("\nTime taken by this Event %0.10Lf\n",timeTE);
printf("\nTheEvent is %d whose sumk(i) is %f \n", TheEvent, Sumk[TheEvent - 1]);
printf("Total Time past is %0.10Lf seconds \n", time);


//HERE IS THE EVENT FLIP

na = Event[TheEvent - 1][1];
nv = Event[TheEvent - 1][2];
time =time + timeTE;
if (FULLfnn[nv -1][9] == -1)
  {

//THE FLIP
   FULLfnn[na - 1][9]= -1;
   FULLfnn[nv - 1][9]=0;

//MSD FOR Cr
xo= Data[nv-1][0];
yo= Data[nv-1][1];
zo= Data[nv-1][2];

if (((Data[na-1][0] - xo) <0) && (fabs(Data[na-1][0] - xo) > ux/2))
   xo= xo - ux;
else if (((Data[na-1][0] - xo) >0) && (fabs(Data[na-1][0] - xo) > ux/2))
   xo = xo + ux;

if (((Data[na-1][1] - yo) <0) && (fabs(Data[na-1][1] - yo) > uy/2))
   yo= yo - uy;
else if (((Data[na-1][1] - yo) >0) && (fabs(Data[na-1][1] - yo) > uy/2))
   yo = yo + uy;

if (((Data[na-1][2] - zo) <0) && (fabs(Data[na-1][2] - zo) > uz/2))
   zo= zo - uz;
else if (((Data[na-1][2] - zo) >0) && (fabs(Data[na-1][2] - zo) > uz/2))
   zo= zo + uz;

SDstepcr= ((pow(Lconst*(Data[na-1][0] - xo),2) + pow(Lconst*(Data[na-1][1] - yo),2) + pow(Lconst*(
SDcr=SDcr+SDstepcr;
fprintf(msdpcr, "%0.10Lf %0.20f\n", time, SDcr);
  }

else
   {

//THE FLIP
```

```
    FULLfnn[na - 1][9]=1;
    FULLfnn[nv - 1][9]=0;


//MSD For Fe
xo= Data[nv-1][0];
yo= Data[nv-1][1];
zo= Data[nv-1][2];

if (((Data[na-1][0] - xo) <0) && (fabs(Data[na-1][0] - xo) > ux/2))
    xo= xo - ux;
else if (((Data[na-1][0] - xo) >0) && (fabs(Data[na-1][0] - xo) > ux/2))
    xo = xo + ux;

if (((Data[na-1][1] - yo) <0) && (fabs(Data[na-1][1] - yo) > uy/2))
    yo= yo - uy;
else if (((Data[na-1][1] - yo) >0) && (fabs(Data[na-1][1] - yo) > uy/2))
    yo = yo + uy;

if (((Data[na-1][2] - zo) <0) && (fabs(Data[na-1][2] - zo) > uz/2))
    zo= zo - uz;
else if (((Data[na-1][2] - zo) >0) && (fabs(Data[na-1][2] - zo) > uz/2))
    zo= zo + uz;

SDstep= ((pow(Lconst*(Data[na-1][0] - xo),2) + pow(Lconst*(Data[na-1][1] - yo),2) + pow(Lconst*(Da
SD=SD+SDstep;
fprintf(msdp, "%0.10Lf %0.20f\n", time, SD);
    }
//MEAN SQUARED DEVIATION CALCULATION
//MSDstep= pow((3*pow((2.83*0.5),2)), 2);

/*printf("%f %f\n", xo, Data[na-1][0]);
printf("%f %f\n", yo, Data[na-1][1]);
printf("%f %f\n", zo, Data[na-1][2]);
printf("%f %f %f\n", fabs(Data[na-1][0] - xo), fabs(Data[na-1][1] - yo), fabs(Data[na-1][2] - zo));*/

//printf("LAttice constant is %f \n", Lconst);
/*printf("After Tranformed : \n");
printf("%f %f \n",xo, Data[na-1][0]);
printf("%f %f \n",yo, Data[na-1][1]);
printf("%f %f \n",zo, Data[na-1][2]);
printf("%f \n", pow(Lconst*(Data[na-1][0] - xo),2));
printf("%f \n", pow(Lconst*(Data[na-1][1] - yo),2));
printf("%f \n", pow(Lconst*(Data[na-1][2] - zo),2)); */

//printf("\nSD taken by this Event %f\n",SDstep);

//printf("Total SD is %f \n", time);


/*printf("..........................................\n");
printf("\nThe First Nearsest Neighbours of all the lattice sites:\n");    //printing FULLfnn
printf("\nConfiguration %d\n\n", step + 1);
   for(l = 0; l < atoms; l++)
      {
        for (m=0; m< 10; m++)
          {
            printf("%d\t", FULLfnn[l][m]);
          }
         printf("\n");
       }

*/

}
for(l = 0; l < nvac*8; l++)
{
        free(Event[l]);
}
free(Event);

fclose(msdp);
}
```

References

[1] The Economist, Q4 (2009).

[2] K. Murthy, I. Charit, Jour. of Nucl. Mater. **383**, 189 (2008).

[3] N. Marzari, *Handbook of Materials Modeling*, (Springer, Dordrecht, 2005).

[4] B.D. Wirth, G.R. Odette, J. Marian, L. Ventelon, J.A. Young-Vandersall, L.A. Zepeda-Ruiz, Jour. of Nucl. Materials **103**, 329 (2004).

[5] W. Kohn, Rev. Mod. Phys. **71**, 1253, (1999).

[6] G. Henkelman, B. P. Uberuaga, H. Jónsson J. Chem. Phys., **113**, 9901 (2000).

[7] G. Henkelman, G. Jóhannesson and H. Jónsson *Theoretical Methods in Condensed Phase Chemistry*, (Kluwer, Dordrecht, 2002).

[8] G. H. Vineyard, J. Phys. Chem. Solids, **3**, 121 (1957).

[9] A. Voter, *Radiation Effects in Solids*, (Springer, 2005).

[10] J. Perdew, K. Burke, M. Ernzerhof, Phy. Rev. Letters **77**, 3865, (1996).

[11] C. Kittel, *Introduction to Solid State Physics, 7ed* (Wiley, New York, 2004)

[12] C. Domain and C. S. Becquart, Phys. Rev. B **65**, 024103 (2001).

[13] C. C. Fu, F. Willaime, P. Ordeján, Phys. Rev. Lett. **92**, 175503 (2004).

[14] P. Olsson, Phy. Rev. B **75**, 14110 (2007).

[15] H. J. Monkhorst and J. Pack, Phy. Rev. B **13**, 5188 (1976).

[16] E. Fawcett, H. L. Alberts, Rev. Mod. Phys. **66**, 25 (1994).

[17] T. P. C. Klaver, Phy. Rev. B **74**, 94435 (2006).

[18] G. Kresse and D. Joubert, Phys. Rev. B **59**, 1758 (1999).

[19] P. E. Blöchl, Phys. Rev. B **50**, 17953 1994.

[20] P. Söderlind, L.H. Yang, J.A. Moriarty, J.M. Wills, Phys. Rev. B. **61**, 2579 (2000).

[21] A. Möslang, H. Graf, G. Balzer, E. Recknagel, A. Weidinger, Th. Wichert, R. I. Grynszpan, Phys. Rev. B **27**, 2674 (1983).

[22] A. Vehanen, P. Hautojärvi, J. Johansson, J. Yli-Kauppila, and P.Moser, Phys. Rev. B **25**, 762 (1982).

[23] H. R. Schober, W. Petry, and J. Trampenau, J. Phys.: Condens. Matter **4**, 9321 (1992).

[24] G. Was, *Fundamental of Radiation Material Science*, (Springer, Berlin, 2007).

[25] P. Olsson, I.A. Abrikosov, L. Vitos, J. Wallenius, J. Nucl. Mater. **321**, 84 (2003).

[26] P. Olsson, I.A. Abrikosov, J. Wallenius, Phys. Rev. B **73**, 104416 (2006).

[27] Daan Frenkel and Berend Smit, *Understanding Molecular Simulation* (Academic Press, San Diego, 1996).

[28] A. D. Le Claire, *Treatise on Physical Chemistry* **10**, 261 (Academic Press, New York, 1970).